Contributions to Mineralogy and Petrology (2021) 176:53
https://doi.org/10.1007/s00410-021-01811-7

ORIGINAL PAPER

Retrograded garnet peridotites from Col des Bagenelles and Crébimont in the Variscan Vosges Mountains (NE France)

Rainer Altherr[1]

Received: 9 January 2021 / Accepted: 9 June 2021 / Published online: 23 June 2021

Abstract

Like the Moldanubian parts of the Bohemian Massif and the French Massif Central, the Vosges Mts (NE France) comprise an uppermost tectonic unit that consists of retrograded (U)H*P*/UH*T* granulites, eclogites and garnet peridotites, originally metamorphosed at pressures of ≥ 4 GPa and temperatures of ≥ 950 °C. Two amphibole–garnet–spinel-bearing peridotite bodies located near to Col des Bagenelles (CB) and Crébimont (CR) show a pronounced retrograde evolution. Primary garnet was completely transformed to a symplectite of orthopyroxene + clinopyroxene + Cr-poor spinel ± amphibole, partially surrounded by a discontinuous outer zone of coarser grains of pyroxenes ± amphibole. Such symplectites are typical for the sliding reaction garnet + olivine ± Na_2O ± K_2O ± H_2O = orthopyroxene + clinopyroxene + spinel ± amphibole. Both peridotites contain 'primary' Cr–Al–spinel. In the sample from CB, such grains occur only within the symplectites after garnet, but never in the matrix, while in the sample from CR, Cr–Al–spinel is present as inclusions within the symplectites and as isolated grains within the surrounding matrix. In the peridotite from CR, that is more depleted than that from CB, these Cr–Al–spinel grains show intense chemical zoning with Cr and Fe^{2+} decreasing, but Al and Mg increasing from core to rim. This pattern is interpreted as retrograde zoning during decompression. Primary *P–T* conditions deduced from compositions of matrix pyroxenes under the assumption of equilibration with earlier garnet are ≥ 1.6–1.7 GPa/ ≥ 900 °C for sample CB, but ≥ 2.3 GPa/ ≥ 860 °C for sample CR. Temperature conditions during the breakdown of garnet are indicated by pyroxenes from the symplectites and are 833 ± 18 (CB) and 812 ± 11 °C (CR) using the Ca-in-Opx thermometer at a chosen pressure of 1.3 GPa.

Keywords Retrograded garnet peridotite · Geothermobarometry · Metamorphic evolution · Variscan orogeny · Vosges Mts

Introduction

Like many other parts of the fragmentarily exposed Variscan orogenic chain in Europe, the Vosges Mts (NE France) contains several tectonic units of polymetamorphic rocks (e.g. Rey et al. 1992; Gardien et al. 1997). In the Moldanubian zone of the Bohemian Massif, the Vosges Mts and the French Massif Central, the uppermost tectonic unit consists of relics of garnet peridotites and eclogites enclosed by felsic gneisses that contain granulite relics. It is now clear that this rock package originated from an ultrahigh-pressure (UH*P*) and ultrahigh-temperature (UH*T*) metamorphic event at conditions of ≥ 4 GPa/ ≥ 950 °C, but suffered variable retrogression during exhumation to mid-crustal levels (e.g. Altherr and Kalt 1996; Berger et al. 2010; Faryad et al. 2011; Massonne 2011; Naemura et al. 2011; Thiéry 2012; Perraki and Faryad 2014; Jedlicka et al. 2015; Haifler and Kotková 2016; Altherr and Soder 2018; Sorger et al. 2018; De Hoÿm de Marien et al. 2020; Vanderhaeghe et al. 2020). Retrogression is the largest in the felsic rocks that often show a UH*P* granulitic stage overprinted by mid-crustal amphibolite-facies metamorphism (Perraki and Faryad 2014; Altherr and Soder 2018). The UH*P* eclogites are often partially or completely transformed to retrogressed mafic granulites or even amphibolites (Hanel et al. 1993). In many cases, garnet peridotite bodies are retrogressed marginally or along shear zones.

In the central part of the Vosges Mts, a number of orogenic garnet peridotite bodies surrounded by felsic gneisses that contain relic granulitic volumes are known (Hameurt 1968; Altherr and Kalt 1996; Gayk and Kleinschrodt 2000;

Communicated by Timothy L. Grove.

✉ Rainer Altherr
rainer.altherr@geow.uni-heidelberg.de

[1] Institute of Earth Sciences, Heidelberg University, Im Neuenheimer Feld 234-236, 69120 Heidelberg, Germany

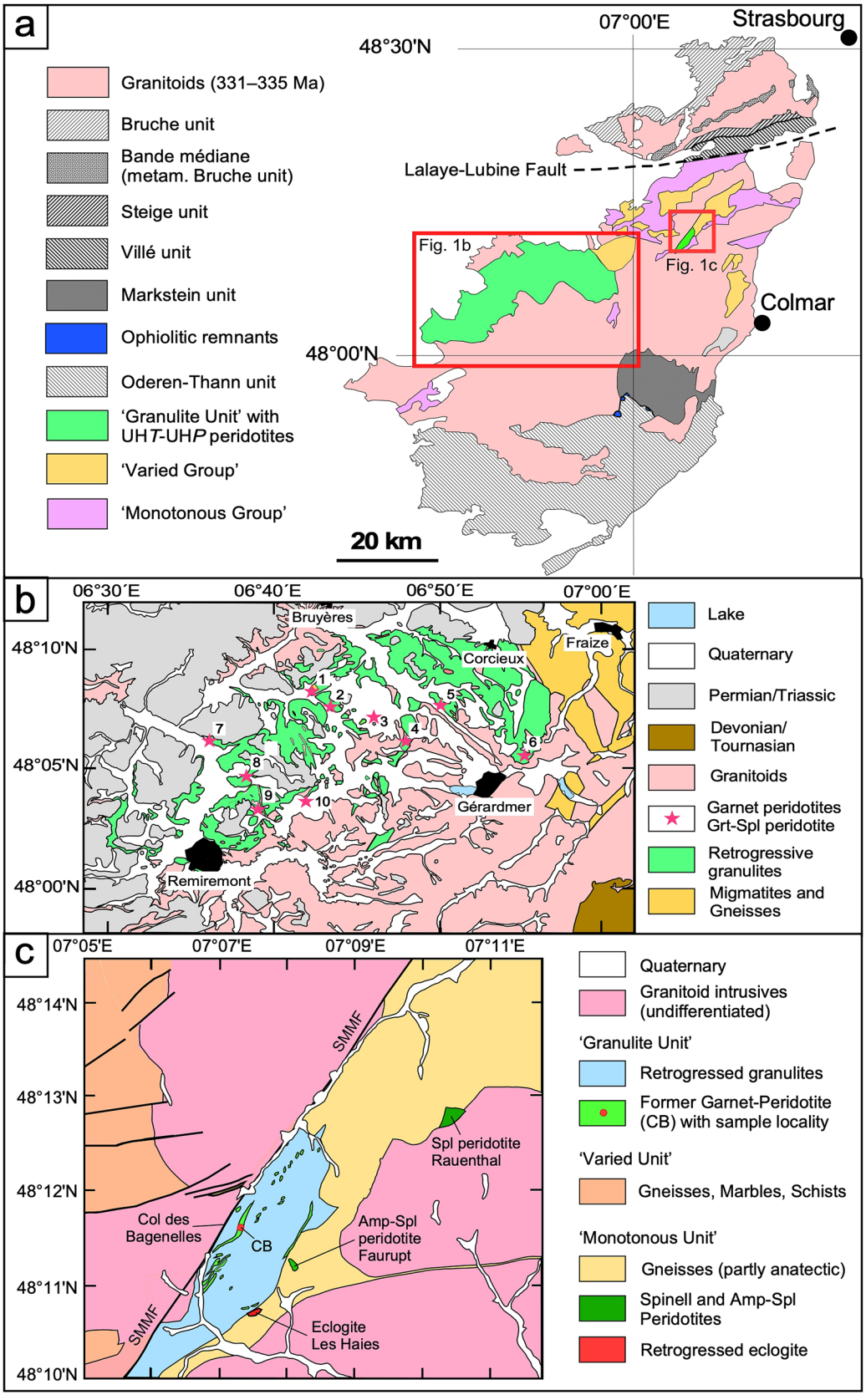
a
Granitoids (331–335 Ma)
Bruche unit
Bande médiane (metam. Bruche unit)
Steige unit
Villé unit
Markstein unit
Ophiolitic remnants
Oderen-Thann unit
'Granulite Unit' with UHT-UHP peridotites
'Varied Group'
'Monotonous Group'
07°00'E
Strasbourg
48°30'N
Lalaye-Lubine Fault
Fig. 1b
Fig. 1c
Colmar
48°00'N
20 km
b
06°30´E
06°40´E
06°50´E
07°00´E
48°10'N
48°05'N
48°00'N
Bruyères
Corcieux
Fraize
Gérardmer
Remiremont
1
2
3
4
5
6
7
8
9
10
Lake
Quaternary
Permian/Triassic
Devonian/ Tournasian
Granitoids
Garnet peridotites Grt-Spl peridotite
Retrogressive granulites
Migmatites and Gneisses
c
07°05'E
07°07'E
07°09'E
07°11'E
48°14'N
48°13'N
48°12'N
48°11'N
48°10'N
SMMF
SMMF
Spl peridotite Rauenthal
Col des Bagenelles
CB
Amp-Spl peridotite Faurupt
Eclogite Les Haies
Quaternary
Granitoid intrusives (undifferentiated)
'Granulite Unit'
Retrogressed granulites
Former Garnet-Peridotite (CB) with sample locality
'Varied Unit'
Gneisses, Marbles, Schists
'Monotonous Unit'
Gneisses (partly anatectic)
Spinell and Amp-Spl Peridotites
Retrogressed eclogite

◂**Fig. 1** **a** Geological sketch map of the Vosges Mts. **b** Geological map of the area with felsic gneisses (retrogressive granulites) containing a small body of former garnet–spinel peridotite (8, Crébimont) and small bodies of former garnet peridotite (1, Laveline-du-Houx; 2, Belle Vue; 3, Champ de Laxet; 4, Col de Perthuis near Liezey; 5, l'Etang d'Oran; 6, Roche des Bruyères; 7, Au Trout Vauthier; 9, La Charme; 10 Flaconnières). **c** Geological map of a part of the Ste-Marie-aux-Mines fault system (SMMF) around the Col des Bagenelles (CB) with tens of small bodies of former garnet peridotite and the location of sample CB

Altherr and Soder 2018). This paper contains a study of two bodies of retrogressed peridotites from Col des Bagenelles (CB) and Crébimont (CR) that are enclosed by felsic gneisses containing granulitic relics. The rock from CB originally was a garnet-peridotite that contains relic primary spinel only as inclusions in former garnet. The CR peridotite, however, has primary spinel occurring not only in former garnet, but also in the surrounding matrix, suggesting an origin as garnet–spinel peridotite. In both rocks, garnet is transformed to a symplectite of orthopyroxene, clinopyroxene and secondary spinel. After a petrographic description of these ultramafic rocks, the results of geothermobarometric calculations are given. These data will be discussed against the background of available *P–T* pseudosections and experimental results. Furthermore, the geodynamic significance of these new data will be discussed within the context of the Variscan collision.

Geological setting

In the central parts of the Vosges Mts, the occurrence of garnet-bearing peridotites is strictly connected with the distribution of amphibolite-facies felsic gneisses that contain granulite relics (Hameurt 1962a, b, 1968; Altherr and Kalt 1996; Gayk and Kleinschrodt 2000; Skrzypek et al. 2012; Lardeaux et al. 2014; Altherr and Soder 2018). This rock association forms a larger mass located between the towns of Remiremont in the SW, Bruyéres and Corcieux in the North, Gérbepal and Xonrupt-Longemer in the East and Gérardmer in the SE (Fig. 1a, b). This area is located to the NW of the large dextral strike slip fault system of Ste-Marie-aux-Mines (SMMF) and contains at least nine larger bodies of garnet peridotite (Hameurt 1968; Altherr and Kalt 1996; Altherr and Soder 2018). In addition, there is one body of retrograde garnet–spinel peridotite, located at Crébimont (CR), about 5 km to the NNE of Remiremont. Towards NNE of Le Bonhomme, the main SMMF passes the Col des Bagenelles and the town of Ste-Marie-aux-Mines further to the NNE (Fig. 1a, c). The former garnet peridotite of Col des Bagenelles (CB) is located a few hundred meters to the ESE of the main SMMF and was most probably displaced towards the NNE by this fault system. For further information see Fluck et al. (1978), Vincent et al. (1985), Altherr and Kalt (1996) and Altherr and Soder (2018).

Sampling and analytical techniques

The sample of the former amphibole–garnet peridotite from Col de Bagenelles was taken about 400 m to the East of the pass (Fig. 1c). Coordinates are 48° 11′ 35″ N/07° 07′ 16″ E (Carte géologique de la France à 1:50000, sheet 341, Gérardmer). The sample of the former garnet–spinel peridotite from Crébimont was taken about 2.7 km SE of Eloyes and 5 km NNE of Remiremont (Fig. 1b). The coordinates are 48° 04' 39' N/06° 38′ 30″ E (Carte géologique de la France à 1:50000, sheet 340, Bruyères).

For bulk-rock analysis, about 1 kg of sample was processed in a steel jaw crusher. After splitting, an aliquot of ~ 80 g was ground in an agate ring-disc mill. The rock powder was then dried at 105 °C for 24 h. Major element concentrations were determined by wavelength dispersive X-ray fluorescence (WDXRF) using lithium borate fusion disks. Abundances of Cr and Ni were also measured by WDXRF using pressed powder tablets. Calibration was done with international reference samples. H_2O was determined by the Karl–Fischer titration method.

Back-scattered electron (BSE) imaging was performed with a LEO 440 scanning electron microscope (SEM) equipped with an Oxford Inca EDX system. Operating conditions were 20 kV and variable sample current.

Mineral analyses were carried out at the Institute of Earth Sciences at Heidelberg University with a Cameca SX51 electron microprobe equipped with five wavelength-dispersive spectrometers. Operating parameters were 15 kV accelerating voltage, 20 nA beam current and a beam diameter of ~ 1 µm. Counting time was 10 s for Fe, Mn, Na and K, 20 s for Si, Al, Mg and Ca and 30 s for Ti and Cr. Natural and synthetic oxide and silicate reference materials were used for calibration. Matrix corrections were performed online with the PAP algorithm (Pouchou and Pichoir 1984, 1985). For detection limits, see Altherr et al. (2013).

Results

Bulk-rock chemistry

Major element bulk-rock chemical compositions of samples CB-118, CR-1 and CR-2 are given in Table 1. Because H_2O contents are high, due to intensive serpentinization and the presence of small amounts of amphibole and chlorite, the recalculated compositions of these peridotites (H_2O free and normalized to 100%) have also been included for comparison with fertile mantle compositions from the literature.

Table 1 Major element bulk-rock analyses of garnet-bearing peridotites from Col de Bagenelles (CB) and from Crébimont (CR) in comparison to fertile peridotites from literature

	Investigated peridotites from the Vosges Mts						Fertile peridotites from literature				
Sample	CB-1	CB-1*	CR-1	CR-1*	CR-2	CR-2*	PM	MPY	KLB-1	KR4003	PY III
SiO_2	39.80	44.78	39.94	45.02	39.86	45.04	45.40	44.74	44.48	44.90	45.20
TiO_2	0.11	0.12	0.05	0.06	0.06	0.07	0.21	0.17	0.16	0.16	0.71
Al_2O_3	2.98	3.35	2.23	2.51	2.06	2.34	4.49	4.37	3.59	4.26	3.54
Cr_2O_3	0.31	0.35	0.45	0.51	0.46	0.52	0.37	0.45	0.31	0.41	0.43
FeO_{tot}	7.63	8.58	7.35	8.29	7.30	8.25	8.10	7.55	8.10	8.02	8.48
MnO	0.14	0.16	0.15	0.17	0.12	0.13	0.14	0.11	0.12	0.13	0.14
MgO	35.23	39.63	36.73	41.41	36.59	41.34	36.77	38.57	39.22	37.3	37.48
NiO	0.24	0.27	0.27	0.30	0.28	0.30	0.24	0.26	0.25	0.24	0.20
CaO	2.28	2.56	1.38	1.56	1.60	1.81	3.65	3.38	3.44	3.45	3.08
Na_2O	0.16	0.18	0.13	0.15	0.16	0.18	0.35	0.40	0.30	0.22	0.57
K_2O	0.01	0.01	0.02	0.02	0.02	0.02	0.03	0.00	0.02	0.09	0.13
P_2O_5	0.01	0.01	0.00	0.00	0.00	0.00	0.02	0.00	0.03	–	–
H_2O	10.39	–	10.75	–	10.93	–	–	0.60	–	–	–
Total	99.29	100.00	99.45	100.00	99.44	100.00	99.77	100.60	100.02	99.18	99.96
Mg#	89.17	89.17	89.90	89.90	89.93	89.93	89.00	90.11	89.62	89.20	88.74
Cr#	6.5	6.5	12.6	12.6	13.0	13.0	5.2	6.5	5.5	6.1	7.5
Ca#	4.0	4.0	2.4	2.4	2.9	2.9	6.0	5.4	5.3	5.6	5.0

*Analyses recalculated to 100.00% (H_2O free)

PM = primitive mantle after Palme and O'Neill (2014), MPY = MORB pyrolite (Niida and Green 1999), KLB-1 (Hirose and Kushiro 1993), KR4003 (Walter 1998), Py III = Pyrolite III (Green and Ringwood 1967). Mg# = 100•molar [MgO/(MgO + FeO_{tot})], Cr# = 100•molar [Cr_2O_3/(Cr_2O_3 + Al_2O_3)] and Ca# = 100• molar [CaO/(CaO + MgO + FeO_{tot})]

Relative to these compositions, all our samples recalculated H_2O free are characterized by significantly lower contents of incompatible elements, such as Na, Ca, Al and Ti, but higher contents of more compatible elements, such as Mg, Fe, Cr and Ni. This indicates a significant depletion of these rocks, although their values of Mg# [= 100•molar MgO/(MgO + FeO_{tot})] are still between 89.17 and 89.93, i.e. only moderately higher than that of the primitive mantle (89.00).

Petrography and mineral chemistry

In the description of peridotite samples, mineral abbreviations as given in Whitney & Evans (2010) and Roman numerals are used to describe different mineral generations. Small letters after the Roman numerals indicate different textural positions. Mineral analyses of the two peridotites (CB and CR) are given in Tables 2 and 3, respectively. Moreover, for the different textural types of Cpx and Opx, the concentration ranges and mean values (± 1σ) of TiO_2 Al_2O_3, CaO and Na_2O are given in Table 4.

Former garnet peridotite at Col des Bagenelles

The peridotite from CB is non-foliated and heavily serpentinized. The rock has a former porphyroblastic texture with larger pseudomorphs after Grt I (up to 2 mm in diameter; no relics of Grt I) enclosed within a fine-grained matrix of Ol I, Opx I and Cpx I, sometimes accompanied by Amp I and later Chl IIIm (Fig. 2a). Although the matrix is completely free of spinel, there are some grains of spinel I occurring as inclusions in symplectite after Grt I.

Abundant pseudomorphs after Grt I consist of a thin, discontinuous outer corona (Opx IIb + Cpx IIb ± Amp IIb) and an inner symplectite formed by elongated grains of Opx IIc + Cpx IIc + Spl IIc ± Amp IIc. These symplectites have a 'domain structure', whereby each of several domains is recognized by constant, but different extinction angles of Opx IIc, Cpx IIc and, if present, Amp IIc under cross-polarized light, indicating that each domain consists of one large crystal of Opx IIc (Fig. 2b–f) with smaller, longitudinal crystals of Cpx IIc that also show one common orientation. In some areas, Amp IIc replaces Cpx IIc. Longitudinal Spl IIc grains occur quite often along the interface between Opx IIc and Cpx IIc or Amp IIc, but these nearly one-dimensional Spl IIc crystals may also continue within one of the two pyroxenes and they may have curved orientations (Fig. 2d–f). Except for their larger grain sizes, these symplectites are mineralogically and texturally similar to the 'type I kelyphite' of Obata and Ozawa (2011) and Obata et al. (2013). Looking at different domains within one former Grt I grain shows that the elongated Cpx IIc and Spl IIc grains tend to be nearly radially oriented around the central parts of the pseudomorphs.

Table 2 Representative mineral analyses of the former garnet peridotite from Col de Bagenelles (CB)

Mineral	Opx I	Opx I	Opx IIb	Opx IIb	Opx IIc	Opx IIc	Cpx I	Cpx I	Cpx IIb	Cpx IIb	Cpx IIc	Cpx IIc	Ol I	Spl I	Spl IIc	Amp I	Amp I	Amp IIb	Amp IIc
Analysis	18–102	18–153	18–6	18–160	18–33	18–29	18–154	18–104	18–164	18–131	18–166	18–172	18–53	18–83	18–38	18–80	18–89	18–7	18–142
SiO_2	56.04	55.28	56.31	55.48	55.82	56.01	53.33	52.29	53.17	52.30	53.56	52.19	40.65	0.00	0.00	43.50	43.42	43.31	43.73
TiO_2	0.05	0.07	0.03	0.05	0.04	0.03	0.31	0.40	0.34	0.34	0.19	0.31	0.00	0.00	0.04	1.50	1.64	1.34	1.29
Al_2O_3	3.11	3.88	2.96	3.82	2.62	3.13	3.62	5.75	4.11	5.60	3.62	5.70	0.01	60.32	61.37	15.36	14.76	15.62	15.09
Cr_2O_3	0.24	0.34	0.19	0.18	0.21	0.13	0.79	0.60	0.92	0.58	0.44	0.55	0.02	8.54	6.86	0.87	1.06	0.73	0.57
Fe_2O_3	0.00	0.00	0.00	0.00	0.00	0.00	0.00	0.00	0.00	0.00	0.00	0.00	0.00	0.66	0.49	0.00	0.00	0.00	0.00
FeO	6.45	6.30	6.71	6.78	6.95	6.70	2.27	2.33	2.35	2.19	1.95	2.10	10.01	9.83	9.50	3.37	3.21	3.22	2.78
MnO	0.17	0.14	0.20	0.11	0.17	0.17	0.06	0.04	0.13	0.07	0.03	0.03	0.19	0.04	0.08	0.17	0.07	0.04	0.04
NiO	n.a	n.a	n.a	n.a	n.a	n.a	n.a	n.a	n.a	n.a	n.a	n.a	0.32	n.a	n.a	n.a	n.a	n.a	n.a
MgO	33.38	33.08	33.11	33.24	33.33	33.44	16.04	15.33	15.83	15.19	16.30	15.27	48.84	20.74	20.87	17.65	17.80	17.67	18.15
CaO	0.56	0.44	0.39	0.45	0.32	0.41	21.78	21.38	22.00	22.00	22.78	22.64	0.01	0.00	0.00	11.90	11.87	11.97	12.27
Na_2O	0.02	0.02	0.00	0.02	0.02	0.01	1.10	1.30	1.22	1.19	0.84	1.08	0.00	0.00	0.00	3.23	3.61	3.27	3.54
K_2O	0.00	0.00	0.00	0.00	0.00	0.00	0.00	0.00	0.00	0.00	0.00	0.00	0.00	0.00	0.00	0.20	0.18	0.22	0.17
Total	100.02	99.55	99.90	100.13	99.48	100.03	99.30	99.42	100.07	99.46	99.71	99.87	100.05	100.13	99.21	97.75	97.62	97.39	97.63
Si	1.934	1.916	1.945	1.915	1.940	1.934	1.942	1.901	1.926	1.902	1.942	1.893	0.998	0.000	0.000	6.149	6.155	6.138	6.175
Ti	0.001	0.002	0.001	0.001	0.001	0.001	0.008	0.011	0.009	0.009	0.005	0.008	0.000	0.000	0.001	0.159	0.174	0.142	0.137
Al	0.126	0.159	0.120	0.155	0.108	0.127	0.155	0.246	0.175	0.240	0.155	0.244	0.000	1.815	1.850	2.559	2.466	2.609	2.512
Cr	0.007	0.009	0.005	0.005	0.006	0.003	0.023	0.017	0.026	0.017	0.013	0.016	0.000	0.172	0.139	0.098	0.119	0.082	0.063
Fe^{3+}	0.000	0.000	0.000	0.000	0.000	0.000	0.000	0.000	0.000	0.000	0.000	0.000	0.000	0.013	0.010	0.000	0.000	0.000	0.000
Fe^{2+}	0.186		0.183	0.194	0.196	0.202	0.193	0.069	0.071	0.071	0.067	0.059	0.064	0.205	0.210	0.203	0.398	0.381	0.382
Mn	0.005	0.004	0.006	0.003	0.005	0.005	0.002	0.001	0.004	0.002	0.001	0.001	0.004	0.001	0.002	0.021	0.009	0.004	0.005
Ni	n.c	n.c	n.c	n.c	n.c	n.c	n.c	n.c	n.c	n.c	n.c	n.c	0.006	n.c	n.c	n.c	n.c	n.c	n.c
Mg	1.717	1.709	1.705	1.710	1.727	1.721	0.871	0.831	0.855	0.824	0.881	0.825	1.787	0.789	0.796	3.720	3.761	3.733	3.822
Ca	0.021	0.016	0.014	0.016	0.012	0.015	0.850	0.833	0.854	0.857	0.885	0.880	0.000	0.000	0.000	1.802	1.802	1.817	1.856
Na	0.002	0.001	0.000	0.001	0.001	0.001	0.078	0.092	0.086	0.084	0.059	0.076	0.000	0.000	0.000	0.885	0.991	0.898	0.970
K	0.000	0.000	0.000	0.000	0.000	0.000	0.000	0.000	0.000	0.000	0.000	0.000	0.000	0.000	0.000	0.036	0.032	0.039	0.031
Total	3.999	3.999	3.991	4.005	4.003	4.001	3.999	4.002	4.006	4.003	3.999	4.007	3.000	3.000	3.000	15.827	15.890	15.844	15.900
X_{Mg}	0.902	0.904	0.898	0.897	0.895	0.899	0.926	0.921	0.923	0.925	0.937	0.928	0.897	0.780	0.789	0.903	0.908	0.907	0.921

n.a. = not analysed; n.c. = not calculated. Formulae were calculated on the basis of 6 oxygen for pyroxenes, 4 oxygen for olivine, 4 oxygen and 3 cations for spinel and 22 oxygen and 2 OH^- for amphibole. Furthermore, a ratio of $Fe^{3+}/(Fe^{2+}+Fe^{3+})=0.00$ was assumed for amphiboles. $X_{Mg}=Mg/(Mg+Fe^{2+})$

Table 3 Representative mineral analyses of the peridotite from Crébimont (CR)

Mineral	Opx I	Opx I	Opx IIb	Opx IIb	Opx IIc	Opx IIc	Cpx I	Cpx I	Cpx IIb	Cpx IIc	Cpx IIc	Ol I	Spl I	Spl I	Spl IIc	Amp I	Amp I	Amp IIb	Amp IIc
Analysis	55–64	55–115	55–99	55–90	55–108	55–80	55–37	55–60	55–112	55–12	55–81	55–30	55–1	55–32	55–75	55–31	55–68	55–91	55–11
SiO_2	56.84	56.36	56.38	55.78	56.39	55.82	53.89	52.87	52.17	53.05	52.41	40.59	0.00	0.00	0.00	44.48	45.26	43.97	44.41
TiO_2	0.11	0.09	0.02	0.09	0.06	0.04	0.13	0.29	0.26	0.30	0.24	0.00	0.09	0.00	0..03	1.28	0.86	1.26	1.32
Al_2O_3	1.66	2.38	2.46	3.21	1.78	3.27	1.40	2.52	3.55	2.29	3.69	0.00	28.70	56.64	62.18	13.86	12.81	14.46	14.17
Cr_2O_3	0.33	0.17	0.31	0.19	0.38	0.19	0.37	0.60	0.43	0.43	0.29	0.00	39.32	10.81	6.28	0.95	1.52	0.63	0.89
Fe_2O_3	0.00	0.00	0.00	0.00	0.00	0.00	0.00	0.00	0.00	0.00	0.00	0.00	2.07	1.11	0.11	0.00	0.00	0.00	0.00
FeO	6.69	6.66	6.59	6.81	6.49	6.99	2.34	2.36	2.49	2.19	2.41	9.91	16.76	11.53	10.13	3.44	3.42	3.77	3.61
MnO	0.07	0.13	0.18	0.22	0.19	0.11	0.09	0.07	0.05	0.03	0.03	0.13	0.05	0.06	0.05	0.05	0.05	0.03	0.06
NiO	n.a	n.a	n.a	n.a	n.a	n.a	n.a	n.a	n.a	n.a	n.a	0.47	n.a	n.a	n.a	n.a	n.a	n.a	n.a
MgO	33.99	33.92	33.80	33.60	34.27	33.74	17.64	16.92	16.73	17.09	16.87	48.67	12.97	19.05	20.55	17.81	18.48	17.87	17.96
CaO	0.37	0.35	0.34	0.34	0.32	0.38	23.43	23.21	23.70	23.94	23.47	0.00	0.00	0.00	0.00	12.42	12.58	12.33	12.61
Na_2O	0.01	0.03	0.02	0.02	0.01	0.01	0.47	0.39	0.24	0.21	0.27	0.00	0.00	0.00	0.00	2.63	2.31	2.78	2.65
K_2O	0.00	0.00	0.00	0.00	0.00	0.00	0.00	0.00	0.00	0.00	0.00	0.00	n.a	n.a	n.a	0.17	0.43	0.15	0.15
Total	100.07	100.09	100.10	100.26	99.89	100.55	99.76	99.23	99.62	99.53	99.68	99.77	99.96	99.20	99.33	97.09	97.72	97.25	97.83
Si	1.961	1.944	1.945	1.924	1.950	1.921	1.962	1.936	1.906	1.937	1.910	0.999	0.000	0.000	0.000	6.317	6.398	6.244	6.269
Ti	0.003	0.002	0.001	0.002	0.002	0.001	0.004	0.008	0.007	0.008	0.007	0.000	0.002	0.000	0.001	0.137	0.091	0.135	0.140
Al	0.067	0.097	0.100	0.130	0.073	0.133	0.060	0.109	0.153	0.099	0.158	0.000	1.016	1.753	1.871	2.320	2.134	2.420	2.358
Cr	0.009	0.005	0.008	0.005	0.010	0.005	0.011	0.017	0.012	0.012	0.008	0.000	0.933	0.224	0.127	0.107	0.169	0.071	0.099
Fe^{3+}	0.000	0.000	0.000	0.000	0.000	0.000	0.000	0.000	0.000	0.000	0.000	0.000	0.047	0.022	0.002	0.000	0.000	0.000	0.000
Fe^{2+}	0.193	0.192	0.190	0.196	0.188	0.201	0.071	0.072	0.076	0.067	0.073	0.204	0.421	0.253	0.216	0.409	0.405	0.448	0.426
Mn	0.002	0.004	0.005	0.006	0.006	0.003	0.003	0.002	0.002	0.001	0.001	0.003	0.001	0.001	0.001	0.006	0.006	0.004	0.007
Ni	n.c	n.c	n.c	n.c	n.c	n.c	n.c	n.c	n.c	n.c	n.c	0.009	n.c	n.c	n.c	n.c	n.c	n.c	n.c
Mg	1.748	1.745	1.738	1.728	1.767	1.731	0.958	0.942	0.911	0.930	0.916	1.786	0.580	0.746	0.782	3.771	3.895	3.783	3.779
Ca	0.014	0.013	0.013	0.013	0.012	0.014	0.914	0.911	0.928	0.937	0.916	0.000	0.000	0.000	0.000	1.890	1.906	1.876	1.908
Na	0.001	0.002	0.001	0.001	0.001	0.001	0.033	0.028	0.017	0.015	0.019	0.000	0.000	0.000	0.000	0.724	0.634	0.765	0.724
K	0.000	0.000	0.000	0.000	0.000	0.000	0.000	0.000	0.000	0.000	0.000	0.000	0.000	0.000	0.000	0.031	0.078	0.027	0.027
Total	3.998	4.004	4.001	4.005	4.009	4.010	4.016	4.005	4.012	4.006	4.008	3.001	3.000	3.000	3.000	15.712	15.716	15.773	15.737
X_{Mg}	0.901	0.901	0.901	0.898	0.904	0.896	0.931	0.927	0.923	0.933	0.926	0.897	0.580	0.747	0.783	0.902	0.906	0.894	0.899

n.a. = not analysed; n.c. = not calculated. Formulae were calculated on the basis of 6 oxygen for pyroxenes, 4 oxygen for olivine, 4 oxygen and 3 cations for spinel and 22 oxygen and 2 OH^- for amphibole. Furthermore, a ratio of $Fe^{3+}/(Fe^{2+}+Fe^{3+})=0.00$ was assumed for amphiboles. $X_{Mg}=Mg/(Mg+Fe^{2+})$

Table 4 Concentration ranges of TiO_2, Al_2O_3, CaO and Na_2O (wt%), mean values and standard deviations (1σ) in brackets of pyroxene generations in the two peridotites from Col des Bagenelles and Crébimont (Vosges Mts)

Mineral	*n*	TiO_2	Al_2O_3	CaO	Na_2O
Col des Bagenelles (CB-118 and CB-119)					
Cpx I	52	0.25–0.48 (0.35 ± 0.05)	3.38–5.75 (4.77 ± 0.59)	20.52–22.75 (21.73 ± 0.44)	1.02–1.50 (1.24 ± 0.10)
Cpx IIb	6	0.34–0.49 (0.41 ± 0.06)	4.22–6.01 (5.23 ± 0.64)	21.86–22.48 (22.06 ± 0.21)	1.02–1.22 (1.11 ± 0.08)
Cpx IIc	34	0.13–0.47 (0.29 ± 0.10)	3.62–5.73 (4.55 ± 0.59)	21.67–23.00 (22.51 ± 0.36)	0.78–1.20 (0.95 ± 0.12)
Opx I	38	0.01–0.10 (0.06 ± 0.02)	3.03–4.00 (3.45 ± 0.25)	0.39–0.58 (0.50 ± 0.05)	0.00–0.06 (0.03 ± 0.01)
Opx IIb	20	0.03–0.11 (0.06 ± 0.02)	2.96–4.55 (3.56 ± 0.36)	0.29–0.60 (0.45 ± 0.07)	0.00–0.05 (0.02 ± 0.01)
Opx IIc	38	0.00–0.06 (0.03 ± 0.02)	2.51–3.13 (2.83 ± 0.15)	0.31–0.48 (0.38 ± 0.04)	0.00–0.04 (0.02 ± 0.01)
Crébimont (CR-155)					
Cpx I	13	0.11–0.29 (0.20 ± 0.05)	1.40–2.57 (2.06 ± 0.34)	23.09–24.06 (23.52 ± 0.29)	0.28–0.50 (0.37 ± 0.07)
Cpx IIb	3	0.26–0.40 (0.33 ± 0.10)	3.38–3.89 (3.47 ± 0.12)	23.42–23.87 (23.56 ± 0.20)	0.22–0.27 (0.26 ± 0.02)
Cpx IIc	14	0.20–0.32 (0.26 ± 0.04)	2.29–3.91 (2.93 ± 0.43)	23.47–24.13 (23.84 ± 0.23)	0.18–0.28 (0.23 ± 0.03)
Opx I	20	0.03–0.14 (0.08 ± 0.03)	1.66–2.38 (1.92 ± 0.22)	0.31–0.43 (0.36 ± 0.03)	0.00–0.04 (0.02 ± 0.01)
Opx IIb	4	0.02–0.09 (0.07 ± 0.03)	2.35–3.21 (2.64 ± 0.39)	0.34–0.38 (0.35 ± 0.02)	0.00–0.02 (0.01 ± 0.01)
Opx IIc	7	0.03–0.08 (0.05 ± 0.02)	1.78–3.27 (2.45 ± 0.47)	0.32–0.38 (0.34 ± 0.02)	0.00–0.03 (0.01 ± 0.01)

n = number of analyses

Some of these pseudomorphs after Grt I still contain inclusions of relict Spl I, while Amp IIc and Chl IIIc are rare.

Representative chemical compositions of the minerals occurring in the CB peridotite are given in Table 2. Clinopyroxene I shows variable compositions indicating poor equilibration within the spatial scale of a thin section (Tables 2 and 4). Because the clinopyroxene grains are very small, it was not possible to measure a chemical profile across these grains, but Al_2O_3 seems to increase from core to rim. X_{Mg} values [= Mg/(Mg + Fe_{tot})] range from 0.911 to 0.935. In contrast, Cpx IIb compositions are more homogeneous and show generally high concentrations of TiO_2 and of Al_2O_3, but intermediate contents of CaO and Na_2O (Table 2). The values of X_{Mg} are nearly constant (0.925–0.928). Finally, Cpx IIc is rather heterogeneous and has relatively high X_{Mg} values (0.925–0.937).

Orthopyroxene I shows a much smaller range of chemical compositions (Tables 2 and 4). Again, rim compositions are somewhat richer in Al_2O_3 than the core compositions. The values of X_{Mg} range from 0.894 to 0.904. Orthopyroxene IIb in the coronae of pseudomorphs after Grt I has similar concentrations of TiO_2 and Na_2O, but somewhat lower contents of Al_2O_3 and CaO. The values of X_{Mg} range from 0.895 to 0.907 and are normal for the Mg# of the bulk rock (Table 1). Orthopyroxene IIc has the lowest Al_2O_3 concentrations of all pyroxenes (Tables 2 and 4).

Olivine I has values of X_{Mg} between 0.893 and 0.901 that are consistent with Mg# values of the bulk rock (Table 1).

Spinel I relics included in the symplectites after Grt I show nearly similar compositions within the range of $^{T}(Mg_{0.76–0.79}Fe^{2+}_{0.21–0.24})\ ^{M}(Al^{3+}_{1.76–1.83}Cr^{3+}_{0.16–0.23}Fe^{3+}_{0.00–0.02})_2O_4$ and have values of X_{Cr} [= Cr/(Cr + Al + Fe^{3+})] that range from 0.082 to 0.116. In contrast, Spl IIc has lower X_{Cr} values of 0.059–0.085 and tends to be richer in Mg and Al, but lower in Fe and Cr, although the differences are small with $^{T}(Mg_{0.78–0.81}Fe^{2+}_{0.19–0.22})\ ^{M}(Al^{3+}_{1.81–1.87}Cr^{3+}_{0.12–0.17}Fe^{3+}_{0.00–0.03})_2O_4$.

Amphibole I (matrix) and Amp IIb and IIc (pseudomorphs after Grt I) have similar compositions and are characterized by high Al_2O_3 (14.3–15.6 wt%) and Na_2O contents (3.18–3.62 wt%), moderate TiO_2 (1.2–1.7 wt%) and variable Cr_2O_3 contents (0.56–1.10 wt%). As typical for peridotitic pargasite, K_2O contents (< 0.25 wt%) are low. The values of $^{A}(Na + K + 2Ca)$ and of $^{C}(Al + Fe^{3+} + Cr^{3+} + 2Ti)$ (both in atoms per formula unit, apfu) define these amphiboles to be pargasite according to the nomenclature of the International Mineralogical Association (Hawthorne et al. 2012). It is remarkable that Na contents per 23 oxygens are very high (0.88–1.00 apfu) for all textural groups of amphibole.

Chlorite III is clinochlore and shows a significant compositional variation depending on its textural position. In the matrix, Chl IIIm is characterized by very low Al, but relative high Fe contents: $^{VI}(Mg_{5.17}Fe^{2+}_{0.51}Mn_{0.02}Fe^{3+}_{0.27}Cr_{0.02}Al_{0.01})\ ^{IV}(Si_{3.69}Al_{0.31})O_{10}(OH)_8$. On the other hand, Chl IIIs in the symplectites after garnet is richer in Al and poorer in Fe: $^{VI}(Mg_{4.94–5.18}Fe^{2+}_{0.51–0.65}Mn_{0.02–0.03}Cr_{0.01–0.02}Al_{0.32–0.49})\ ^{IV}(Si_{3.43–3.63}Al_{0.57–0.37})O_{10}(OH)_8$. Hence, the difference between Chl III compositions is clearly controlled by the effective bulk compositions.

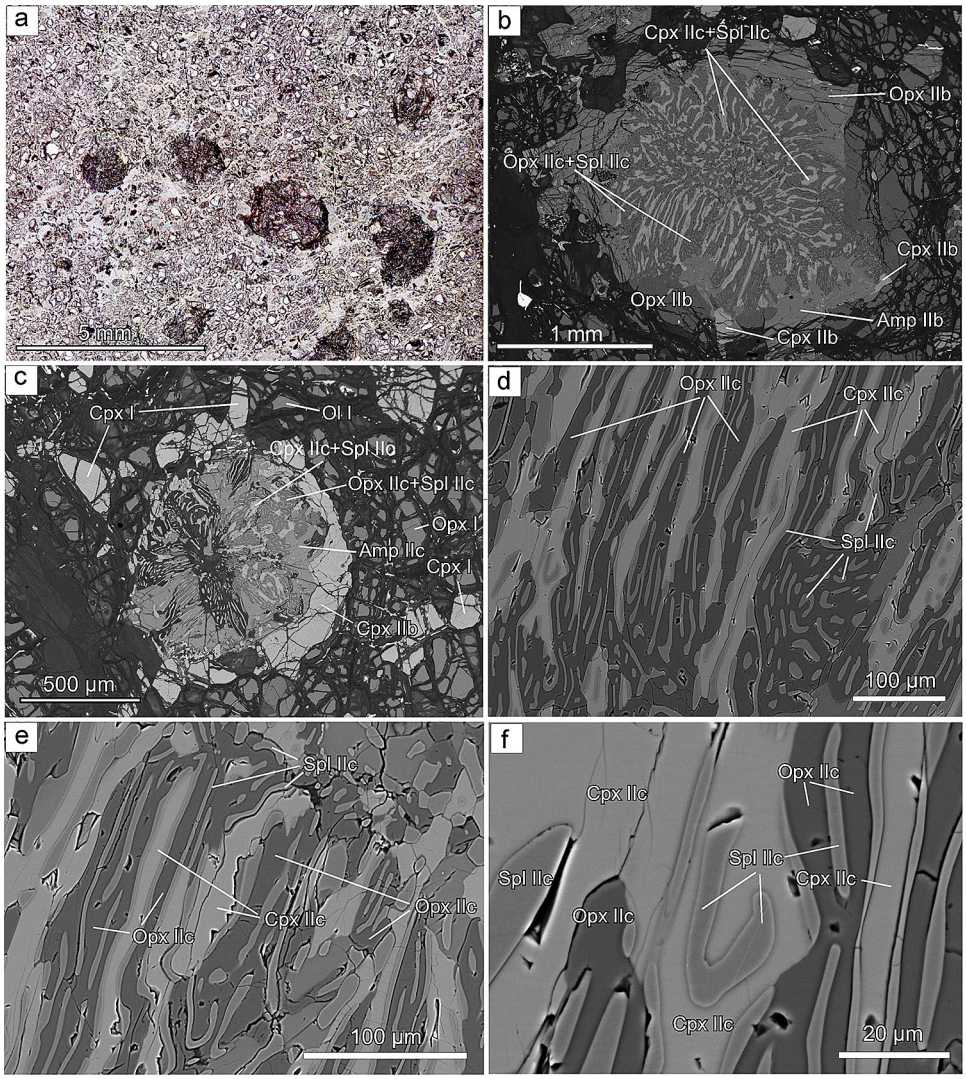

Fig. 2 Petrographic details of the former garnet peridotite from Col des Bagenelles (CB). **a** Part of a thin section with pseudomorphs after garnet and heavily serpentinized fine-grained matrix of Ol I, Opx I and Cpx I. **b** Pseudomorph after Garnet I consisting of a symplectite of Opx IIc, Cpx IIc and Spl IIc, surrounded by a rim of Opx IIb, Cpx IIb and Amp IIb. **c** Pseudomorph after Grt I with rim of Cpx IIb. **d** and **e** Parts of symplectites of Opx IIc, Cpx IIc and Spl IIc after Grt I. **f** Detail of symplectite after Grt I. Note the structure of Sp IIc within Opx IIc and Cpx IIc and along the boundaries between pyroxenes

Former garnet–spinel peridotite from Crébimont

The former garnet–spinel peridotite from CR is heavily serpentinized and contains roundish symplectites of Cpx IIb/c, Opx IIb/c, Spl IIc and Amp IIb/c after Grt I (< 1 mm in diameter) that are texturally similar to those of the peridotite from CB (Fig. 3a, e–f). In marked contrast to the rock from Col des Bagenelles, however, this peridotite also contains Spl I grains that occur not only as inclusions in former Grt I (Spl Ib; Fig. 3b, c), but also as larger matrix grains surrounded by primary Ol I, Opx I, Cpx I and rare Amp I (Spl Ia; Fig. 3d). Moreover, Ol I was rarely found as an inclusion in symplectite after Grt I.

Orthopyroxene I is characterized by low Al_2O_3 contents (1.66–2.74 wt%) that increase from core to rim of the grains (Tables 3 and 4; Fig. 4a), while SiO_2 decreases slightly (Fig. 4b). Mg# values decrease almost imperceptibly from core to rim (Fig. 4c). The concentration of Cr_2O_3 (0.09–0.43 wt%) shows relatively large variation that seems to be controlled by the neighboring phases. In Fig. 4d, the left-hand side of the Opx I profile borders serpentine (former olivine), while the right-hand side borders relatively Cr-rich Spl I. Opx IIb and IIc grains inside the pseudomorphs after Grt I have higher Al_2O_3 concentrations (2.32–3.27 wt%), but similar CaO and Na_2O contents than Opx I (Tables 3 and 4).

Clinopyroxene I is characterized by very low contents in Al_2O_3 (1.40–2.57 wt%; increasing from core to rim of the grains), while Cpx IIb has high Al_2O_3 contents (3.38–3.89 wt%) and Cpx IIc is in between with 2.29–3.91 wt% (Tables 3 and 4). Furthermore, Na_2O is the highest in Cpx I and similarly low in Cpx IIb and IIc. Since Cpx I grains are generally rather small (< 30 µm) we could only measure one very short chemical profile with 13 analyses. In this profile, Si and Na decrease but Al and Ti increase from core to rim (Fig. 5).

Spinel I grains are solid solutions of the endmember components Chromite, Magnesiochromite, Hercynite and Spinel (Bosi et al. 2019), whereby their cores are richer in Cr

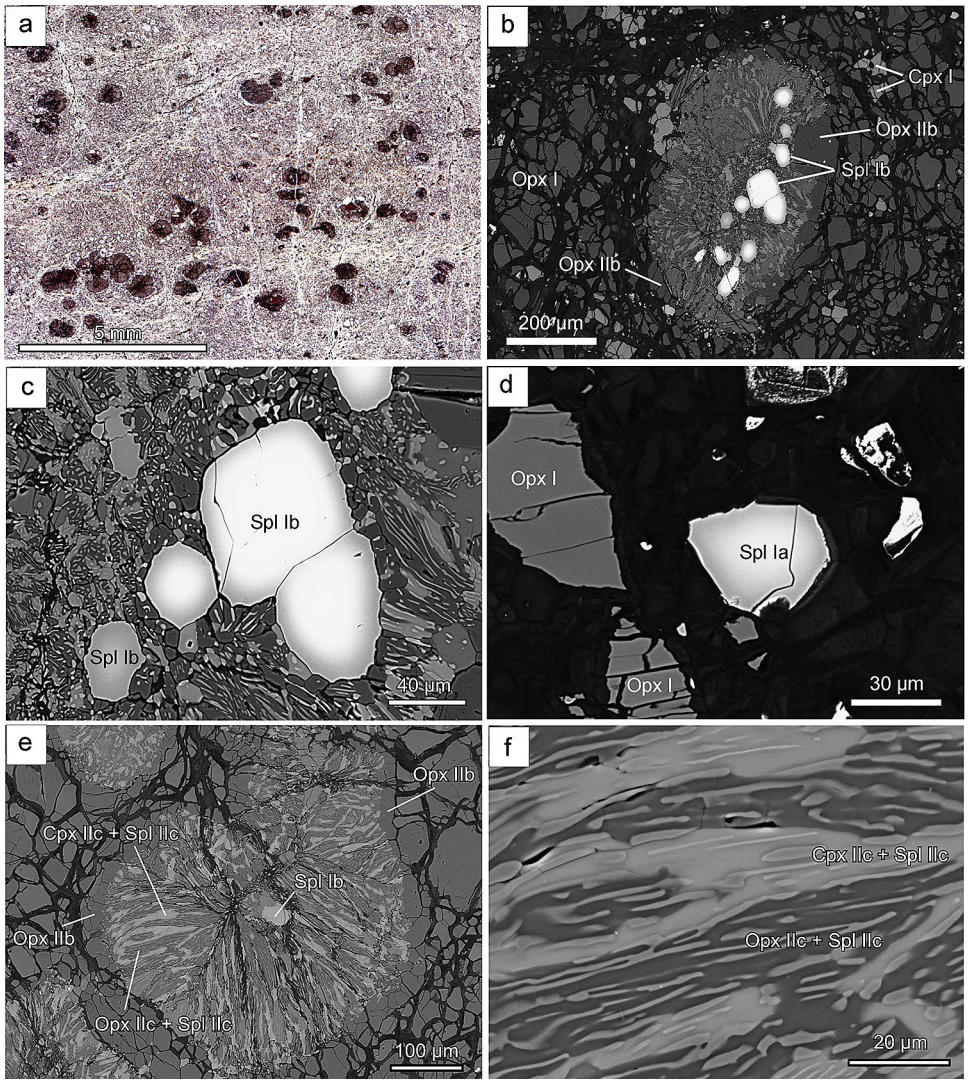

Fig. 3 Petrographic details of the former garnet–spinel peridotite from Crébimont (CR). **a** Part of a thin section with pseudomorphs after garnet and heavily serpentinized fine-grained matrix of Ol I, Opx I and Cpx I. **b** Relict Spl Ib grains within a symplectite after Grt I. **c** Detail of (b) with zoned crystals of Spl Ib within symplectite after Grt I. **d** Spl Ia and Opx I relics within the matrix (dark). **e** Pseudomorph after Grt I with symplectites of Opx IIc, Cpx IIc and Spl IIc as well as Opx IIb at the outer rim. In the core region, relict Spl Ib is visible. **f** Detail of symplectite after Grt I with Opx IIc, Cpx IIc and Spl IIc

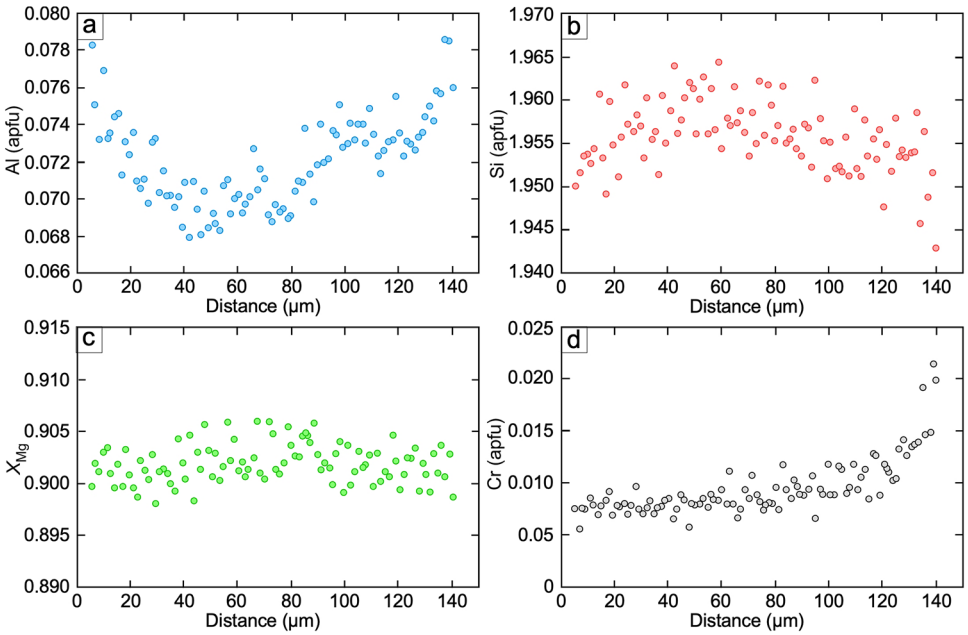

Fig. 4 Compositional profiles across Opx I (rim to rim) of sample CR155 (Crébimont). Left-hand contact is to former Ol I (converted into serpentine), while the right-hand side borders relatively Cr-rich Spl Ia. **a** Al ($=^{IV}Al+^{VI}Al$) in apfu. **b** Si (apfu). **c** $X_{Mg}=Mg/(Mg+Fe_{tot})$ in atomic proportions. **d** Cr (apfu). The influence of Cr-rich Spl Ia at the right-hand marginal zone is clearly visible

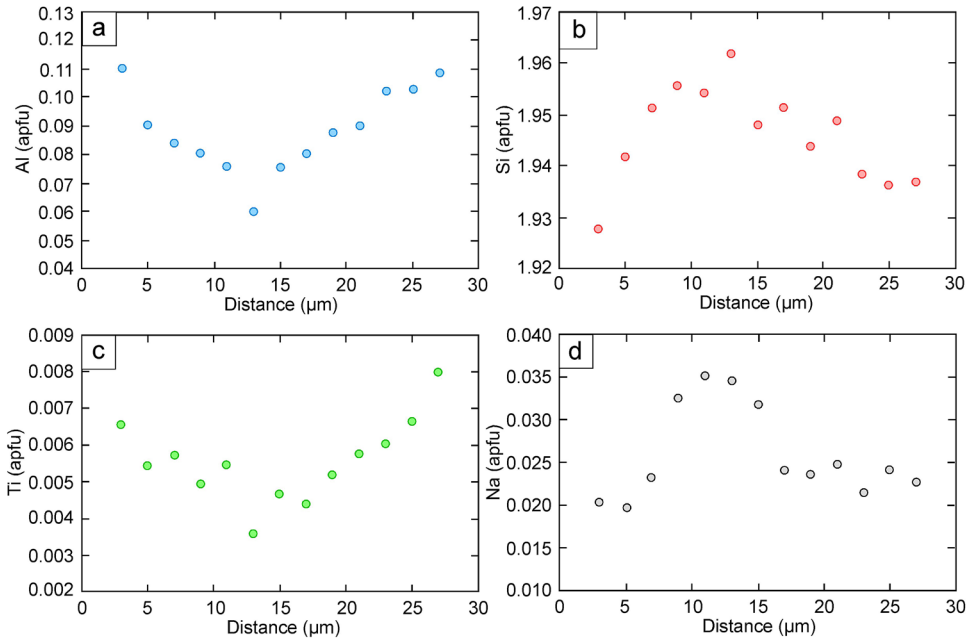

Fig. 5 Compositional profile across a relict Cpx I grain (rim to rim) of sample CR155 (Crébimont). **a** Al (=^{IV}Al + ^{VI}Al) in apfu. **b** Si (apfu). **c** Ti (apfu). **d** Na (apfu)

and Fe^{2+}, while their rims show a strong increase in Al and Mg (Fig. 6; Table 3). Calculated $Fe^{3+}/(Fe^{2+} + Fe^{3+})$ ratios range from 0.074 to 0.140 and the values of X_{Cr} are high and decrease from core to rim of larger grains (0.478 to 0.112). The compositional range is $^{T}(Mg_{0.55–0.76}Fe^{2+}_{0.24–0.44})\ ^{M}(Al^{3+}_{1.00–1.75}Cr^{3+}_{0.22–0.95}Fe^{3+}_{0.02–0.05})O_4$. In marked contrast, Spl IIc grains from the pseudomorphs after Grt I show generally low X_{Cr} values of 0.057 to 0.086 and are characterized by the compositional range $^{T}(Mg_{0.79–0.83}Fe^{2+}_{0.17–0.22})\ ^{M}(Al^{3+}_{1.80–1.87}Cr^{3+}_{0.11–0.17}Fe^{3+}_{0.00–0.05})O_4$, i.e. they are richer in Al and Mg, but poorer in Cr and Fe^{2+} than Spl I grains.

Amphibole I, IIb and IIc grains have pargasitic compositions (Table 3). Relative to amphibole from sample CB, they are characterized by somewhat lower contents of TiO_2 (0.86–1.40 wt%), Al_2O_3 (12.8–14.7 wt%) and Na_2O (2.31–2.80 wt%). These amphiboles have generally lower contents of Na contents per 23 oxygens (Amp I: 0.63–0.72 apfu; Amp IIb and IIc: 0.72–0.77 apfu) than those of peridotite CB.

In this sample, only Chl IIIs was found. It is clinochlore with the compositional range of $^{VI}(Mg_{4.71–5.10}Fe^{2+}_{0.50–0.71}Mn_{0.02–0.04}Cr_{0.01–0.04}Al_{0.25–0.47})^{IV}(Si_{3.61–3.84}Al_{0.39–0.16})O_{10}(OH)_8$.

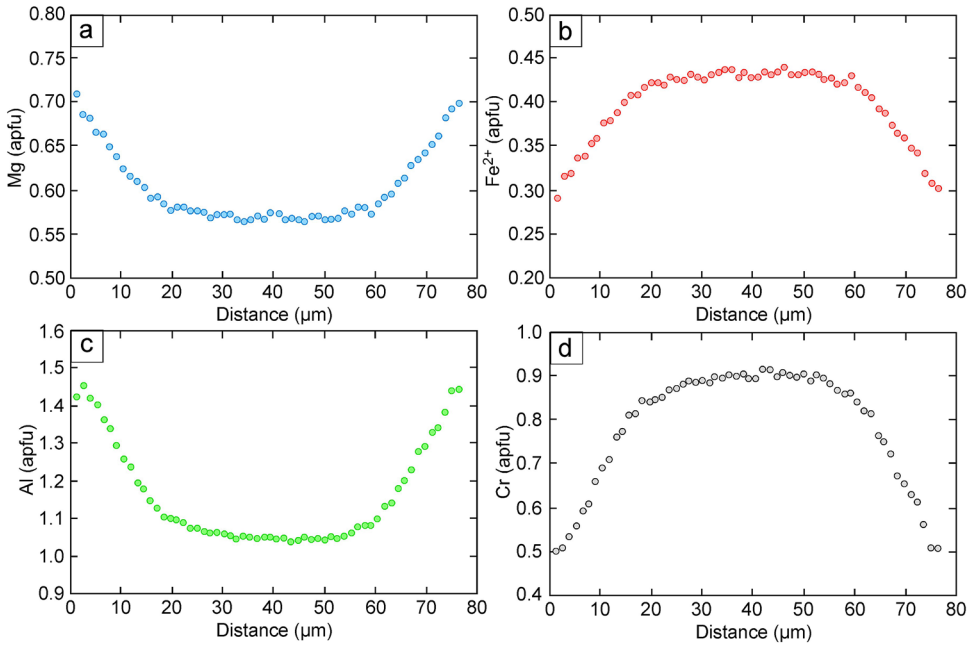

Fig. 6 Compositional profile across a larger Spl Ib grain of sample CR155 (Crébimont). A core-to-rim increase in Mg **(a)** and Al **(c)** is balanced by a decrease in Fe^{2+} **(b)** and Cr **(d)**

Discussion

Occurrence of pargasitic amphibole

Given the relatively large size of Amp I grains in the matrix of the two investigated peridotite bodies and the fact that there are no relevant reaction textures, it can be speculated that Amp I was formed relatively early, before the breakdown of Grt I. Maximum *P–T* conditions of amphibole in peridotite are strongly dependent on bulk-rock composition. For a MORB pyrolite composition (MPY, Table 1), a maximum equilibration pressure of 3.2 GPa (at 925 °C) and temperature of 1080 °C (at ~ 2.3 GPa) have been found experimentally (Niida and Green 1999).

The existence of Amp I in the matrix of both peridotites (CB and CR) indicates the early presence of H_2O in these rock systems. At elevated pressures (> 1.5 GPa) a H_2O-rich fluid phase will, however, dissolve significant amounts of Na, K, Si and Al, and this may hinder the crystallization of amphibole in peridotitic systems with high H_2O contents. In fact, it was shown by Green et al. (2014) that at 2.5 GPa, amphibole is only stable at bulk H_2O contents between about 0.02 and 2.90 wt%. At low H_2O contents of about 0.02–0.4 wt%, this water is present in nominally anhydrous minerals (NAMs) and pargasitic amphibole, but at higher H_2O contents in the system, there is vapour present. Therefore, the solidus temperature of pargasite-bearing lherzolite at ~ 2.5 GPa depends on the amount of H_2O and decreases from the 'dry' solidus (~ 1100 °C) via water-deficient to vapour-saturated conditions at ~ 1020 °C. In a *P–T* field, the wet solidus (> 0.4 wt% H_2O) starts at 10^5 Pa and ~ 1070 °C with a negative slope, turns to a positive slope at about 1 GPa/970 °C and meets the nominally dry solidus (~ 0.02–0.4 wt% H_2O stored in NAMs and pargasite) at ~ 3.2 GPa (Green et al. 2014: Fig. 6).

The occurrence of Amp IIb and IIc demonstrates that free H_2O was available during decompression and replacement of Grt I. This fluid phase was again responsible for the transport of Na, K and perhaps also Si and Al into the growing symplectites.

With increasing pressure and temperature, pargasitic amphibole in peridotite shows increasing contents of Na (Niida and Green 1999: Fig. 8B). In both peridotites investigated in this study, there is no difference in composition among the different generations of amphibole (I, IIb, IIc). Na contents (apfu) calculated by assuming $Fe^{2+}/(Fe^{2+} + Fe^{3+}) = 1$ are clearly different with 0.88–1.00 apfu for peridotite CB, but 0.63–0.77 apfu for CR. It was shown that the isolines of Na contents (apfu) in Amp have a negative slope in the *P–T* field and show increasing Na contents with increasing *P* and *T* (Niida and Green 1999). The difference in Na contents between the amphiboles of both peridotites, however, may also be strongly controlled by the amount of a water-rich fluid phase during amphibole crystallization.

Different roles of spinel I in both peridotites

The most important difference between the two investigated peridotites is the textural position of primary spinel I. In the peridotite from CB, this phase occurs only as a rare inclusion in former Grt I (not shown) but is never in contact with Opx I and Cpx I. Values of X_{Cr} are between 0.082 and 0.116. These facts argue for a relict nature of Spl I and therefore these grains are remnants of the prograde formation of garnet + olivine from orthopyroxene + clinopyroxene + spinel. This situation is comparable to the Nonsberg region in the Alps, where the garnets of the 'coarse-type peridotites' also show relict spinel inclusions caused by a transformation of spinel lherzolite to garnet lherzolite (Obata and Morten 1987).

In marked contrast to the CB peridotite, Spl I in the peridotite CR occurs not only included in Grt I (called Spl Ib; Fig. 3c), but also as an additional phase in the matrix far away from former Grt I, but in contact with Opx I and Cpx I (called Spl Ia; Fig. 3d). Moreover, both Spl Ia and Ib grains show the same type of core-to-rim zoning (decreasing X_{Cr} from ~ 0.48 to 0.11). Such a situation is a strong argument in favour of a spinel–garnet peridotitic origin of this rock. The strong chemical zoning of both, Spl Ia and Ib grains (Fig. 6) is retrograde and mainly due to a decompression rather than a decrease in temperature.

P–T conditions of the spinel–garnet peridotite field in fertile compositions

In the subsolidus part of the lherzolite system, the sliding reaction

$$\mathrm{Grt} + \mathrm{Ol} \pm \mathrm{H_2O} \pm \mathrm{Na_2O} \pm \mathrm{K_2O} = \mathrm{Opx} + \mathrm{Cpx} + \mathrm{Spl} \pm \mathrm{Amp} \quad (1a)$$

separates the garnet peridotite field at higher pressures from the spinel peridotite field at lower pressures for a given temperature (Fig. 7). The shape and *P–T* size of the intermediate spinel to garnet peridotite transition interval, however, is poorly known due to the lack of sufficient thermodynamic data on Cr-bearing mineral endmembers (Klemme 2004; Klemme et al. 2000, 2009; Ziberna et al. 2013; Holland et al. 2018; Tomlinson and Holland 2021). Experiments in the system SMACCr showed that the influence of Cr on the garnet-in boundary is not linear, since small amounts of Cr shift this boundary strongly towards higher pressures. For example, at 1000 °C, the garnet-in boundary is at ~ 1.6 GPa

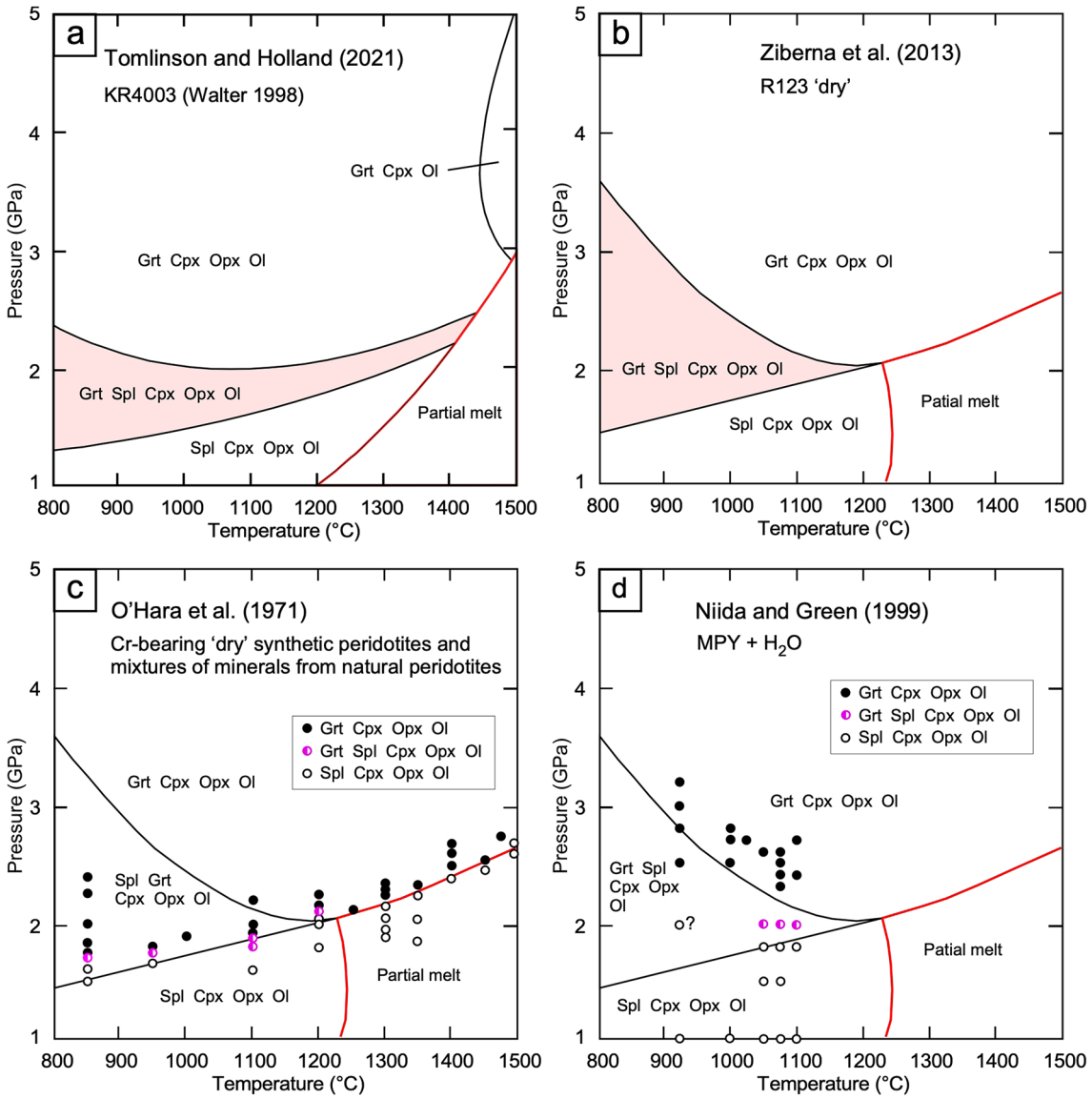

Fig. 7 **a** *P–T* Pseudosection for peridotite KR4003 (Walter 1998) modified after Tomlinson and Holland (2021). **b** *P–T* pseudosection for peridotite R123 after Ziberna et al. (2013). For a petrographic and chemical description of this peridotite see Frey et al. (1985). **c** Results of experiments on fertile peridotites by O'Hara et al. (1971). Paragenesis of garnet peridotite, spinel–garnet peridotite and spinel peridotite are marked by different symbols. Intermediate spinel–garnet peridotite is only stable within a narrow pressure band. **d** Results of experiments on the fertile, water-bearing peridotite MPY by Niida and Green (1999). See Table 1 for composition and text for further explanation. In **c** and **d**, the phase boundaries of lherzolite R123 as calculated by Ziberna et al. (2013) are given for orientation

for a Cr-free system, but at 1.9 GPa for a system with Cr# = 5 [Cr# = 100•molar (Cr_2O_3/(Cr_2O_3 + Al_2O_3))]. However, at higher values of Cr# this curve flattens considerably and for Cr# = 10 it is at about 2.1 GPa (Nickel 1986).

Fertility of peridotites can be expressed by two values of their bulk-rock compositions. Fertile peridotites are characterized by high contents of Al_2O_3 and CaO. Thus, their Cr# value should be rather low (< 7) and their Ca# value [= 100•molar (CaO/(CaO + MgO + FeO_{tot}))] should be relatively high (> 4). For fertile compositions such as KLB-1 (Takahashi 1986; Zhang and Herzberg 1994) with Cr# = 5.5 and Ca# = 5.3 or KR4003 (Walter 1998) with Cr# = 6.1 and Ca# = 5.6, revised *P–T* pseudosections were published by Holland et al. (2018) and Tomlinson and Holland (2021), respectively. In the diagram of Tomlinson and Holland (2021) (Fig. 7a), the relatively thin intermediate *P–T* field of the spinel–garnet transition starts as a thin band at the solidus at ~ 2.4 GPa/1425 °C and widens towards lower *P–T* values, whereby the spinel-out boundary becomes concave upward, while the garnet-in boundary has always a positive slope. The widening of the garnet–spinel peridotite field towards lower temperature is

thought to be strongly sensitive to the contents of ferric iron and chromium in the bulk system (Holland et al. 2018; Tomlinson and Holland 2021).

Using different thermodynamic data, Ziberna et al. (2013) published a *P–T* pseudosection for their system R123 (Cr# = 4.1, Ca# = 6.7) that is slightly more fertile than KLB-1 and KR4003 (Fig. 7b). This pseudosection has a larger wedge-shaped spinel–garnet lherzolite field than the pseudosection of KR4003 (Tomlinson and Holland (2021).

Given the actual situation with the uncertainty of thermodynamic data for Cr-bearing spinel and other relevant phases (e.g. Klemme and O'Neill 2000; Klemme et al. 2000, 2009; Klemme 2004), it seems reasonable to look at experimental work with suitable peridotitic bulk compositions in order to solve the inconsistency concerning the stability of spinel–garnet peridotite (Fig. 7a, b). MacGregor (1970) was the first who experimentally demonstrated the importance of the Cr# value of the bulk composition and he also proposed that an increasing value of Cr# resulted in a higher pressure of the relatively small transition field of spinel–garnet peridotite. Green and Ringwood (1967) carried out experiments on 'dry', relatively fertile Cr-bearing peridotite compositions ("Pyrolite III"; Table 1) at pressures of 1.8–4.0 GPa and temperatures of 1100–1600 °C. They found that "garnet and spinel coexist together over a very small pressure interval" at *P–T* conditions just on or above a line from 2.0 GPa/1050 °C to 2.5 GPa/1440 °C.

O'Hara et al. (1971) used 'dry' synthetic peridotites and mixtures from natural (i.e. Cr bearing) peridotites (plagioclase, spinel or garnet bearing) and got a narrow boundary field ($\Delta P \approx 0.1$ GPa) between spinel and garnet peridotite, running from about 1.65 GPa/850 °C via 1.8–1.9 GPa/1100 °C to 2.1 GPa/1200 °C (Fig. 7c; O'Hara et al. 1971: Fig. 4). Interestingly enough, five runs of their experiments at 850, 950, 1100 and 1200 °C yielded 'newly formed' garnet + spinel assemblages, so there is the possibility to interpret these data as a proof for a narrow stability field (small ΔP) of garnet–spinel peridotite even at low *T* values (< 1000 °C). These experiments also show that garnet peridotite (without Spl) may be stable at very low pressures suggested by Fig. 7a (Tomlinson and Holland 2021). Fan et al. (1997) used mineral separates from a natural spinel peridotite and their experiments ('dry') showed that garnet + spinel are stable at 1.8–2.0 GPa/1100 °C and 2.5 GPa/1150 °C. These results are nearly similar to those of O'Hara et al. (1971).

The experiments of Niida and Green (1999) were carried out with a MORB pyrolite composition that contained variable amounts of H_2O (Cr# value of 6.5; MPY in Table 1). It was found that garnet was present in all experiments at *P–T* conditions ≥ 2.0 GPa and 925–1100 °C (Fig. 7d). Furthermore, they found coexisting garnet + spinel only at 2.0 GPa and 1050–1100 °C. There is only one experiment (at 2.5 GPa/925 °C) that yielded garnet peridotite without spinel. These *P–T* conditions are located in the spinel–garnet peridotite field of Ziberna et al. (2013) (Fig. 7d). There is, however, another experiment at 2.0 GPa/925 °C, that yielded spinel (without garnet?), which is somehow in conflict with the results of the other three experiments at 2.0 GPa/1050–1100 °C that yielded garnet + spinel.

Despite the unfortunate situation, that 'dry' experiments at temperatures below about 1100 °C in lherzolite systems may show misleading results due to sluggish equilibration, it is thought that a relatively small ΔP value (~ 1 GPa) of the spinel–garnet peridotite field at 800 °C (Fig. 7a) is more likely correct than a value of more than 2 GPa (Fig. 7b). In any case, the reason for this large difference between both models should be further investigated.

P–T evolution of the investigated peridotites

The primary phase assemblages of the investigated peridotites were changed by decompression to the assemblage of an amphibole–spinel peridotite:

$$\text{Grt I} + \text{Ol I} \pm \text{H}_2\text{O} \pm \text{Na}_2\text{O} \pm \text{K}_2\text{O} = \text{Opx IIb/c} + \text{Cpx IIb/c} + \text{Spl IIb/c} \pm \text{Amp IIb/c} \quad (1b)$$

For relatively fertile peridotite compositions this means that the final *P–T* conditions of the garnet-free peridotites were below pressures of ~ 1.3–1.4 GPa at 800–1000 °C (Tomlinson and Holland 2021). During decompression of garnet-bearing peridotites, continued chemical diffusion between Grt and Ol in the field of garnet–spinel peridotite may be stopped after the symplectitic shell of Opx, Cpx and Spl around relic Grt has gained a certain width. In such a case, the further garnet consuming reaction

$$\text{Grt} \pm \text{Na}_2\text{O} = \text{Opx} + \text{Cpx} + \text{Plg (An} - \text{rich)} + \text{Spl} \quad (2)$$

may occur at lower pressures than reaction (1a) (Kushiro and Yoder 1966; Obata 2011). However, despite a careful search, no plagioclase was found in symplectites after Grt I in both investigated samples, so it is assumed that garnet was completely consumed by reaction (1a). Thus, the rare relics of Ol I occurring as inclusions in the symplectites have to be interpreted as relics after reaction (1a). Most probably, the efficiency of reaction (1a) was increased by the early presence of H_2O in the reacting volumes, as indicated by rare Amp IIc and Chl IIc within the symplectites.

After their original equilibration as garnet (CB) and garnet–spinel (CR) peridotite, the two investigated rocks were subject to retrogression leading to the complete consumption of garnet by the sliding reaction (1a). This reaction was due to decompression (Fig. 7a). The garnet peridotite CB (Spl I is only present as rare inclusions in Grt I) was transformed to a rock with two chemical subsystems, corresponding to (i) former pyrope-rich garnet transformed by reaction with

olivine and a H_2O-rich fluid (containing Na and K) into a corona of Opx IIb + Cpx IIb and an inner symplectite of Opx IIc + Cpx IIc + Spl IIc ± Amp IIc, whereby Spl IIc is relatively rich in Al and Mg, but poor in Cr and Fe and (ii) the Mg-rich, but Al-poorer matrix consisting originally of Ol I + Opx I + Cpx I. Both the relatively large chemical heterogeneity of Cpx I and Opx I (Table 4) and the presence of presumably younger Amp IIa indicate, that the minerals of the first generation (I) may have changed their original chemical compositions to a certain degree. Moreover, there was some chemical exchange between the matrix and the symplectitic 'pseudomorphs' after Grt I.

The former garnet–spinel peridotite from Crébimont (CR) preserved its Spl Ia and Ib in both the matrix and the former Grt I domains, but also gained additional Spl IIc due to the sliding reaction (1b). Furthermore, former Spl Ia and Ib grains characterized by relatively high X_{Cr} changed their composition to less Cr-rich rims at the lower boundary of the garnet–spinel peridotite field, compatible with a decompression. The influence of the bulk rock Cr# value on X_{Cr} of spinel and garnet in peridotite is given by a partly schematic P–X_{Cr} section in Fig. 8 (Webb and Wood 1986; Brey et al. 1991; Klemme 2004; Grütter et al. 2006; Fumagalli et al. 2014; Lakey 2019). The pressure width ΔP of the garnet–spinel peridotite stability field is strongly dependent on the value of Cr# of the system. In relatively fertile bulk-rock compositions, such as that of sample CB (Cr# = 6.5; Table 1), the sub-assemblage garnet + spinel is only stable within a small ΔP range (~ 1 GPa), while this assemblage in sample CR (Cr# = 12.6–13.0; Table 1) would be stable up to very high pressure (6–7 GPa; Fig. 8). As can be seen schematically, a relatively small decrease in P (i.e. from ~ 2.6 to 1.8 GPa) will be able to explain the observed pronounced zoning of Spl Ia/Ib in CR, while the Cr# value of Grt I decreased only slightly.

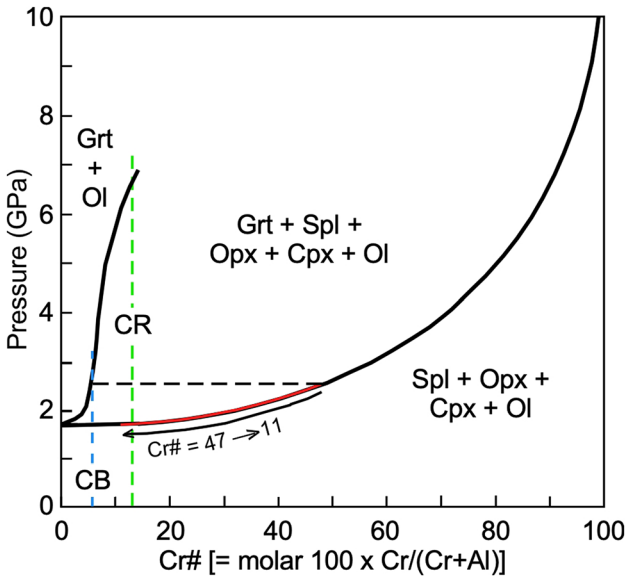

Fig. 8 Semiquantitative P-Cr# pseudosection (at about 900 °C) for garnet–spinel peridotite CR and garnet peridotite CB, constructed after experimental data of Webb and Wood (1986), Brey et al. (1991), Klemme (2004), Grütter et al. (2006), Fumagalli et al. (2014) and Lakey (2019). Green and blue dashed vertical lines stand for bulk-rock compositions of peridotites CR and CB, respectively. Phase boundaries of garnet + olivine, garnet + spinel + orthopyroxene + clinopyroxene + olivine and spinel + orthopyroxene + clinopyroxene + olivine are given (heavy black lines). The range of Spl Ia and Ib compositions in sample CR is given with core-to-rim zoning (red line and black arrow). This chemical zonation of spinel grains is consistent with a decompression. For further explanation see sub-chapter 'P–T evolution of the investigated peridotites'

Geothermobarometry

Geothermobarometry on unequilibrated peridotites that contain clear petrographic evidence for changing P–T conditions, such as those investigated in this paper is problematic. Moreover, even for equilibrated peridotites there may be problems resulting from the use of simplified chemical compositions for experimental calibration of thermobarometers. For example, the often-used two-pyroxene thermometry (e.g. Brey and Köhler 1990) may be biased by high Na contents in the pyroxenes (Brey and Köhler 1990; Nimis and Grütter 2010). In the case of the CR peridotite with Na-in-Cpx < 0.04 apfu, this problem is practically non-existent, but for the CB peridotite with Na-in-Cpx = 0.06–0.11 apfu, this would probably cause significant differences. Another problem concerns thermometers that are based on Mg–Fe^{2+} partitioning between garnet and pyroxenes, since it has been shown that the presence of Fe^{3+} in these phases may influence the calculated temperatures significantly (e.g. Matjuschkin et al. 2014; Nimis et al. 2015).

Given the chemical heterogeneities of Opx I and Cpx I in both samples, any attempts to use geothermobarometry for deducing their primary P–T states are problematic. In particular, it is not clear in which way and to which degree these pyroxenes changed their compositions during the retrograde evolution by which Grt I was completely consumed during decompression and an eventual concomitant decrease in temperature. The only way to proceed is to use the Ca-in-Opx geothermometer of Brey and Köhler (1990) in combination with the Al-in-Opx barometers of Brey and Köhler (1990) and Nickel and Green (1985). Although garnet is no longer present in the investigated peridotites, a model garnet composition for pressure calculations is used. This composition corresponds to the composition of 'grt 07' from the garnet peridotite of Laveline-du-Houx (Vosges Mts) given by Altherr and Soder (2018: Table 1). This procedure is justified because (i) variations in garnet compositions within fertile peridotite systems are rather limited in the P–T range of 2–6 GPa and 700–1100 °C and (ii) Al-in-Opx barometers

are not very sensitive to garnet composition (e.g. Altherr and Kalt 1996). It is, however, clear that Opx I and Cpx I grains show a significant zoning, in particular in sample CR (Fig. 4), with Al_2O_3 contents increasing from core to rim, suggesting either significant heating and/or a decompression during growth of these pyroxenes.

First, the thermobarometric results on sample CB (former garnet peridotite) will be discussed. Applying the Al-in-Opx barometer in combination with the Ca-in-Opx thermometer of Brey and Köhler (1990) on Opx I core analyses yielded mean *P–T* values of 1.61 ± 0.18 GPa and 891 ± 28 °C (1σ; $n = 26$). If the Al-in-Opx barometer of Nickel and Green (1985) is used, similar *P–T* values of 1.70 ± 0.19 GPa and 895 ± 28 °C (1σ) are obtained. The pressure dependence of the Ca-in-Opx thermometer is about 40 °C/GPa. Furthermore, temperature values calculated with the two-pyroxene thermometer of Brey and Köhler (1990) are also similar with 868 ± 59 °C (1σ; $n = 78$) for an assumed pressure value of 1.65 GPa. For this thermometer, the pressure dependence is only 14 °C/GPa. All the *P–T* conditions obtained for Opx I are thus clearly located in the garnet–spinel peridotite field (Fig. 7a), suggesting that the Al concentration in Opx I was increased during pressure release, even in the cores of the grains.

In order to get some more information on the temperature at which the final breakdown of garnet in peridotite CB happened, the compositions of coexisting Cpx IIc and Opx IIc in the symplectites after Grt I can be used. Application of the Ca-in-Opx thermometer of Brey and Köhler (1990) for 1.3 GPa yields an average *T* value of 833 ± 18 °C (1σ, $n = 27$), while the two-pyroxene thermometer (Brey and Köhler 1990) yields 814 ± 55 °C (1σ, $n = 31$). Both temperature values are similar and indicate some cooling during decompression and garnet breakdown.

The former garnet–spinel peridotite CR is more depleted, since it has lower contents of Al_2O_3 and CaO, but higher contents of Cr_2O_3 (Table 1). Although pervasive secondary serpentinization prevents a determination of the primary mode, the low contents of CaO suggest that the rock was probably a harzburgite with less than 5% modal clinopyroxene. This means that we cannot really use the *P–T* pseudosection for the KR4003 composition that is lherzolitic, since in more depleted compositions the field for garnet–spinel peridotite may be broader than that of the fertile lherzolite KR4003. Both, Opx I and Cpx I of CR have lower Al contents than the pyroxenes of peridotite CB and both pyroxenes even show a more pronounced core-to-rim increase in Al (Figs. 4a and 5a) consistent with a decompression. Using core compositions for both pyroxenes, the combination of the Al-in-Opx barometer with the Ca-in-Opx thermometer yields *P–T* values of 2.3 ± 0.3 GPa and 857 ± 22 °C (Brey and Köhler 1990). The two-pyroxene thermometer of Brey and Köhler (1990) yields a lower temperature value of 804 ± 39 °C.

For a pressure of 1.3 GPa consistent with the final breakdown of Grt I, the symplectitic pyroxenes IIc of sample CR yield a Ca-in-Opx temperature of 812 ± 11 °C (1σ, $n = 7$) and a two-pyroxene temperature of 763 ± 32 °C (1σ, $n = 14$). It has to be noted, that the boundary between the spinel peridotite and the garnet–spinel peridotite fields always has a moderate positive slope in the *P–T* field, whereby this boundary may move to higher pressures with increasing peridotite depletion and Cr# value (Ziberna et al. 2013).

Secondary nature of chlorite III

In both samples, chlorite III occurs as a retrograde phase, but formed relatively early after formation of the assemblage Grt I + Opx I + Cpx I + Amp I ± Spl I. The high-temperature stability limit of chlorite (clinochlore) in garnet peridotite systems is given by the reaction.

$$\text{Chlorite} + \text{Orthopyroxene} = \text{Garnet} + \text{Olivine} + H_2O. \quad (3)$$

At high pressure, this reaction has a steep negative slope (Pawley 2003; Fumagalli and Poli 2005; Fumagalli et al. 2014; Lakey 2019) and terminates at an invariant point at ~ 2.3 GPa/850 °C (Lakey 2019). From this invariant point, the chlorite breakdown reaction

$$\text{Chorite} = \text{Orthopyroxene} + \text{Olivine} + \text{Spinel} + H_2O \quad (4)$$

starts with a positive slope and terminates at the transition from plagioclase to spinel peridotite at 0.8 GPa/800 °C (Lakey 2019). In the former garnet peridotite CB, Chl IIIm occurs in the matrix and has relatively low Al_2O_3 contents reflecting the bulk composition of the matrix outside Grt I.

Geodynamic consequences and speculations

It has been shown that most of the peridotites in the uppermost tectonic unit of the Moldanubian zone in the French Massif Central, the Vosges Mts and the Bohemian Massif are UH*P* garnet peridotites that were generated at *P–T* conditions of ≥ 4 GPa and 1000–1100 °C (e.g. Gardien et al. 1988, 1990; Altherr and Kalt 1996; Medaris et al. 2003, 2005, 2006, 2009; Lardeaux 2014; Altherr and Soder 2018; Muriuki et al. 2020). These rocks form relatively small bodies and are often closely associated with UH*P* eclogite. Both UH*P* metamorphic rock types are enclosed within felsic gneisses that were retrogressively formed from H*P* granulites. Since the latter may contain relict coesite and microdiamond inclusions in zircon and garnet (Lardeaux et al. 2001; Perraki and Faryad 2014), they also had a UH*P* past. Furthermore, Naemura et al. (2011) described a diamond

inclusion in Cr-spinel of the spinel–garnet peridotite from Plešovice (Blanský Les Massif in the SW Czech Republic). This observation shows that even 'equilibrated' spinel–garnet peridotites may have a UH*P* past. During rapid transport towards the Earth's surface at high temperatures, the reactivity of a certain rock volume will depend on a number of characteristics, such as, for example, grain size, ductility, degree of deformation, chemical composition and water content. It is clear, that acid to intermediate (U)H*P* metamorphic rocks are more ductile than 'dry' peridotite and eclogite and this easily explains the fact, that the latter rock types are more resistant to retrogression than the felsic rocks. Moreover, exhumation of high-density peridotite and eclogite is always difficult and; therefore, such rock volumes need a relatively light transport medium such as the felsic granulites or their UH*P* precursor rocks in which they can be carried to shallower depths.

So far, we did not find any signs of a possible UH*P* past of the two 'garnet-bearing' peridotites (CB and CR) described in this study. This could either mean that these rocks never were at depths of more than ~ 70 km or that their mineralogical past was already completely erased during transport towards the Earth's surface. In any case, the 'negative density jump' at the Moho (ultramafic rocks below vs mafic rocks above) reduced the buoyancy of the exhuming rock package of light felsic rocks enclosing minor volumes of peridotite and UH*P* eclogite. Additionally, minor amounts of water entered these rocks and enhanced partial transformation of the garnet peridotites to amphibole–spinel peridotites. Another possibility is, that the two investigated peridotites formed partial volumes in the outer zones of an ascending mass of rocks and were therefore more heavily deformed and also more extensively overprinted by an ingress of water which produced not only the chemical retrogression of pyroxenes I, but also caused crystallization of amphibole I.

Conclusions

The two investigated peridotite bodies CB and CR bear clear evidence for their exhumation within a larger mass of felsic gneisses (relict granulites). Both peridotites contain zoned symplectites that attest the former presence of garnet. This phase was completely eliminated by the sliding reaction garnet + olivine ± H_2O ± Na_2O ± K_2O = orthopyroxene + clinopyroxene + spinel ± amphibole. While the more fertile peridotite CB contains only some grains of relict spinel that once formed inclusions within garnet, the more depleted peridotite CR has abundant older Cr–Al–spinel grains that are zoned and occur in both the symplectites after garnet and the matrix. The more depleted CR peridotite therefore was a spinel–garnet peridotite. According to its bulk rock Cr#, Cr–Al spinel in this peridotite would be stable to ultrahigh pressures of 6–7 GPa.

Water was always present in the rocks during their exhumation, since amphibole occurs in the matrix and in the symplectites after garnet. Therefore, it is well possible that 'primary' *P*–*T* conditions were significantly higher than 1.6–1.7 ± 0.2 GPa/890 ± 30 °C for CB and 2.3 ± 0.3 GPa/869 ± 20 °C for CR. These conditions are significantly lower than those determined for the other garnet peridotites of the central Vosges Mts (≥ 4.0 GPa/≥ 1000 °C; Altherr and Kalt 1996; Altherr and Soder 2018). For the (final) breakdown of garnet, a pressure of 1.3 GPa was assumed in accord with experimental evidence. Temperatures obtained from pyroxenes of the symplectites are 830 ± 20 °C (CB) and 810 ± 10 °C (CR).

A rapid decompression as suggested by the textures and mineral compositions of the two investigated peridotites seems only possible by their enclosure within low-density rocks such as the present felsic granulite relics and gneisses. Nevertheless, the rapid ascent of this rock package was temporarily slowed down by the negative density jump at the Moho. Moreover, ductility of the rocks could have changed due to cooling.

Acknowledgements Thanks are due to Angelika Kalt for her companionship during field work. Moreover, I acknowledge help by Hans-Peter Meyer during electron microprobe analyses. Moreover, Stephan Klemme and Christian Soder are thanked for fruitful discussions. Michael Hanel critically read the manuscript and gave valuable suggestions. Last but not the least, the paper was improved by constructive criticisms from "MO" and an anonymous reviewer.

Funding This research did not receive any specific grant from funding agencies in the public, commercial or non-for-profit sectors.

Declarations

Conflict of interest The authors declare that they have no known competing financial interests or personal relationships that could have appeared to influence the work reported in this paper.

References

Altherr R, Kalt A (1996) Metamorphic evolution of ultrahigh-pressure garnet peridotites from the Variscan Vosges Mts. (France). Chem Geol 134:27–47

Altherr R, Soder CG (2018) Sapphirine as a breakdown product of garnet in a Variscan UHP/HT peridotite from the Vosges Mountains (France)—an indication of near-isothermal decompression. J Petrol 59:2221–2243. https://doi.org/10.1093/petrology/egy096

Altherr R, Soder C, Panienka S, Peters D, Meyer H-P (2013) Pink manganian phengite in a high *P*/*T* meta-conglomerate from northern Syros (Cyclades, Greece). Contrib Mineral Petrol 166:1323–1334. https://doi.org/10.1007/s00410-013-0929-7

Berger J, Féménias O, Ohnenstetter D, Bruguier O, Plissart G, Mercier J-C, Demaiffe D (2010) New occurrence of UHP eclogites

in Limousin (French Massif Central): age, tectonic setting and fluid-rock interactions. Lithos 118:365–382. https://doi.org/10.1016/j.lithos.2010.05.013

Bosi F, Biagioni C, Pasero M (2019) Nomenclature and classification of the spinel supergroup. Eur J Mineral 31:183–192. https://doi.org/10.1127/ejm/2019/003-2788

Brey GP, Köhler T (1990) Geothermobarometry in four-phase lherzolites II. New thermobarometers, and practical assessment of existing thermobarometers. J Petrol 31:1353–1378

Brey G, Doroshev A, Kogarko L (1991) The join pyrope-knorringite: experimental constraints for a new geothermobarometer for coexisting garnet and spinel. 5th International Kimberlite Conference, Brazil, Extended Abstracts, 26–28

Fan Q, Liu R, Xie H, Zhang Y, Xu P, Lin Z (1997) Experimental study of spinel-garnet transition in upper mantle and its significance. Sci China Series D 40:383–389

Faryad SW, Racek M, Lexa O (2011) Eclogite, garnet peridotite, garnet pyroxenite and HP granulite in the Gföhl Unit. Geolines 23:106–111

Fluck P, Ménillet F, Hameurt J, von Eller J-P, Zinglé J-B, Ménillet F, Théobald N, Flageollet J-C, Darmois-Théobald M, Knierim A, Stoehr J, Vogt H (1978) Carte géologique de la France à 1/50.000, sheet Gérardmer. Ministère de l'Industrie, Service Géologique National

Frey FA, Suen CJ, Stockman HW (1985) The Ronda high temperature peridotite: geochemistry and petrogenesis. Geochim Cosmochim Acta 49:2469–2491

Fumagalli P, Poli S (2005) Experimentally determined phase relations in hydrous peridotites to 6.5 GPa and their consequences on the dynamics of subduction zones. J Petrol 46:555–578. https://doi.org/10.1093/petrology/egh088

Fumagalli P, Poli S, Fischer J, Merlini M, Gemmi M (2014) The high-pressure stability of chlorite and other hydrates in subduction mélanges: experiments in the system Cr_2O_3–MgO–Al_2O_3–SiO_2–H_2O. Contrib Mineral Petrol 167:979. https://doi.org/10.1007/s00410-014-0979-5

Gardien V, Lardeaux J-M, Misseri M (1988) Les péridotites des Monts du Lyonnais (M.C.F.): témoins privilégiés d'une subduction de lithosphere paleozoique. C R Acad Sci Paris Série II 307:1967–1972

Gardien V, Tegyey M, Lardeaux J-M, Misseri M, Dufour E (1990) Crust-mantle relationships in the French Variscan chain: the example of the Southern Monts du Lyonnais unit (eastern French Massif Central). J Metamorph Geol 8:477–492

Gardien V, Lardeaux J-M, Ledru P, Allemand P, Guillot S (1997) Metamorphism during late orogenic extension: insights from the French Variscan belt. Bull Soc Géol France 168:271–286

Gayk T, Kleinschrodt R (2000) Hot contacts of garnet peridotites in middle/upper crustal levels: new constraints on the nature of the late Variscan high-T/low-P event in the Moldanubian (Central Vosges/NE France). J Metamorph Geol 18:293–305

Green DH, Ringwood AE (1967) The stability fields of aluminous pyroxene peridotite and garnet peridotite and their relevance in upper mantle structure. Earth Planet Sci Lett 3:151–160

Green DH, Hibberson WO, Rosenthal A, Kovács I, Yaxley GM, Falloon TJ, Brink F (2014) Experimental study of the influence of water on melting and phase assemblages in the upper mantle. J Petrol 55:2067–2096. https://doi.org/10.1093/petrology/egu050

Grütter H, Latti D, Menzies A (2006) Cr-saturation arrays in concentrate garnet compositions from kimberlite and their use in mantle barometry. J Petrol 47:801–820. https://doi.org/10.1093/petrology/egi096

Haifler J, Kotková J (2016) UHP–UHT conditions and near-adiabatic exhumation path of diamond-bearing garnet–clinopyroxene rocks from the Eger Crystalline Complex, North Bohemian Massif. Lithos 248–251:366–381. https://doi.org/10.1016/j.lithos.2016.02.001

Hameurt J (1967a) Les terrains cristallins et cristallophylliens du versant occidental des Vosges moyennes. Mémoires Du Service De La Carte Géologique D'alsace Et De Lorraine 26:1–386

Hameurt J (1967b) Carte géologique et pétrographique des terrains cristallins et cristallophylliens des Vosges moyennes Lorraines 1:100,000. Bull Serv Carte Géol Alsace Lorraines 20:117–128

Hameurt J (1968) Les péridotites des Vosges moyennes. Bull Serv De La Carte Géplogique D'alsace Et De Lorraine 21:177–218

Hanel M, Lippolt HJ, Kober B, Wimmenauer W (1993) Lower Carboniferous granulites in the Schwarzwald basement near Hohengeroldseck (SW-Germany). Naturwissenschaften 80:25–28

Hawthorne FC, Oberti R, Harlow GE, Maresch WV, Martin RF, Schumacher JC, Welch MD (2012) Nomenclature of the amphibole supergroup. Am Mineral 97:2031–2048. https://doi.org/10.2138/am.2012.4276

Hirose K, Kushiro I (1993) Partial melting of dry peridotites at high pressures: determination of compositions of melts segregated from peridotite using aggregates of diamond. Earth Planet Sci Lett 114:477–489

Holland TJB, Green ECR, Powell R (2018) Melting of peridotites through to granites: a simple thermodynamic model in the system KNCFMASHTOCr. J Petrol 59:881–900. https://doi.org/10.1093/petrology/egy048

Hoÿm De, de Marien L, Pitra P, Cagnard F, Le Bayon B (2020) Prograde and retrograde P-T evolution of a Variscan high-temperature eclogite, French Massif Central. Haut-Allier. BSGF Earth Sci Bull 191:14. https://doi.org/10.1051/bsgf/2020016

Jedlicka R, Faryad SW, Hauzenberger C (2015) Prograde metamorphic history of UHP granulites from the Moldanubian Zone (Bohemian Massif) revealed by major element and Y + REE zoning in garnets. J Petrol 56:2069–2088. https://doi.org/10.1093/petrology/egv066

Klemme S (2004) The influenc of Cr on the garnet–spinel transition in the Earth's mantle: experiments in the system MgO–Cr_2O_3–SiO_2 and thermodynamic modelling. Lithos 77:639–646. https://doi.org/10.1016/j.lithos.2004.03.017

Klemme S, O'Neill HSC (2000) The effect of Cr on the solubility of Al in orthopyroxene: experiments and thermodynamic modelling. Contrib Mineral Petrol 140:84–98

Klemme S, O'Neill HSC, Schnelle W, Gmelin E (2000) The heat capacity of $MgCr_2O_4$, $FeCr_2O_4$, and Cr_2O_3 at low temperatures and derived thermodynamic properties. Am Mineral 85:1686–1693

Klemme S, Ivanic TJ, Connolly JAD, Harte B (2009) Thermodynamic modelling of Cr-bearing garnets with implications for diamond inclusions and peridotite xenoliths. Lithos 112(Suppl 2):986–991. https://doi.org/10.1016/j.lithos.2009.05.007

Kushiro I, Yoder HS (1966) Anorthite-Forsterite and Anorthite-Enstatite reactions and their bearing on the basalt–eclogite transformation. J Petrol 7:337–362

Lakey SL (2019) Chlorite stability in the subduction zone – Implications for water transport to the deep mantle, slab diapirs and mantle melting. PhD thesis, The Australian National University, 210

Lardeaux J-M (2014) Deciphering orogeny: a metamorphic perspective. Examples from European Alpine and Variscan belts. Part II: Variscan metamorphism in the French Massif Central—a review. Bull Soc Géol France 185:281–310

Lardeaux J-M, Ledru P, Daniel I, Duchene S (2001) The Variscan French Massif Central—a new addition to the high pressure metamorphic 'club': exhumation processes and geodynamic consequences. Tectonophysics 332:143–167

Lardeaux J-M, Schulmann K, Faure M, Janoušek V, Lexa O, Skrzypek E, Edel JB, Štípská P (2014) The Moldanubian Zone in

the French Massif Central, Vosges/Schwarzwald and Bohemian Massif revisited: differences and similarities. Geol Soc London Spec Publ 405:7–44. https://doi.org/10.1144/SP405.14 (**In: Schulmann K, Martínez Catalán JR, Lardeaux JM, Janou Janoušek V, Oggiano G (eds) The Variscan Orogeny: extent, timescale and the formation of the european crust**)

MacGregor ID (1970) The effect of CaO, Cr_2O_3, Fe_2O_3 and Al_2O_3 on the stability of spinel and garnet peridotites. Phys Earth Planet Interiors 3:372–377

Massonne H-J (2011) Occurrences and *PT* conditions of high and ultrahigh pressure rocks in the Bohemian Massif. Geolines 23:18–26

Matjuschkin V, Brey GP, Höfer HE, Woodland AB (2014) The influence of Fe^{3+} on garnet–orthopyroxene and garnet–olivine geothermometers. Contrib Mineral Petrol 167:1–10. https://doi.org/10.1007/s00410-014-0972-z

Medaris LG, Wang HF, Jelínek E, Jakeš P (2003) Garnet peridotite in the Moldanubian Zone in the Czech Republic—a heat source for Variscan metamorphism? J Czech Geol Soc 48:92–93

Medaris G, Wang H, Jelínek E, Mihaljevič M, Jakeš P (2005) Characteristics and origins of diverse Variscan peridotites in the Gföhl Nappe, Bohemian Massif, Czech Republic. Lithos 82:1–23. https://doi.org/10.1016/j.lithos.2004.12.004

Medaris LG, Beard BL, Jelínek E (2006) Mantle-derived, UHP garnet pyroxenite and eclogite in the Moldanubian Gföhl Nappe, Bohemian Massif: a geochemical review, new P-T determinations, and tectonic interpretation. Int Geol Rev 48:765–777

Medaris G, Ackerman L, Jelínek E, Toy V, Siebel W, Tikoff B (2009) The Sklené garnet peridotite: petrology, geochemistry, and structure of a mantle-derived boudin in Moldanubian granulite. J Geosci 54:301–323. https://doi.org/10.3190/jgeosci.052

Muriuki J, Nakamura D, Hirajima T, Svojtka M (2020) Mineralogical heterogeneity of UH*P* garnet peridotite in the Moldanubian Zone of the Bohemian Massif (Nové Dvory, Czech Republic). J Mineral Petrol Sci 115:1–20. https://doi.org/10.2465/jmps.190126

Naemura K, Ikuta D, Kagi H, Odake S, Ueda T, Ohi S, Kobayashi T, Svoitka M, Hirajina T (2011) Diamond and other possible ultradeep evidence discovered in the orogenic spinel–garnet peridotite from the Moldanubian Zone of the Bohemian Massif, Czech Republic. In: Dobrzhinetskaya LF, Faryad SW, Wallis S, Cuthbert S (eds) Ultrahigh-pressure metamorphism. Elsevier Inc., Amsterdam, pp 77–111. https://doi.org/10.1016/B978-0-12-385144-4.00002-3

Nickel KG (1986) Phase equilibria in the system SiO_2-MgO-Al_2O_3-CaO-Cr_2O_3 (SMACCr) and their bearing on spinel/garnet lherzolite relationships. N Jb Miner Abh 155:259–287

Nickel KG, Green DH (1985) Empirical geothermobarometry for garnet peridotites and implications for the nature of the lithosphere, kimberlites and diamonds. Earth Planet Sci Lett 73:158–170

Niida K, Green DH (1999) Stability and chemical composition of pargasitic amphibole in MORB pyrolite under upper mantle conditions. Contrib Mineral Petrol 135:18–40

Nimis P, Grütter H (2010) Internally consistent geothermometers for garnet peridotites and pyroxenites. Contrib Mineral Petrol 159:411–427. https://doi.org/10.1007/s00410-009-0455-9

Nimis P, Goncharov A, Ionov DA, McCammon C (2015) Fe^{3+} partitioning systematics between orthopyroxene and garnet in mantle peridotite xenoliths and implications for thermobarometry of oxidized and reduced mantle rocks. Contrib Mineral Petrol 169:6. https://doi.org/10.1007/s00410-014-1101-8

O'Hara MJ, Richardson SW, Wilson G (1971) Garnet-peridotite stability and occurrence in curst and mantle. Contrib Mineral Petrol 32:48–68

Obata M (2011) Kelyphite and symplectite: Textural and mineralogical diversities and universality, and a new dynamic view of their structural formation. In: Sharkov EV (ed) New frontiers in tectonic research—general problems, sedimentary basins and island arcs. InTech, Rijeka, pp 93–122

Obata M, Morten L (1987) Transformation of spinel lherzolite to garnet lherzolite in ultramafic lenses of the Austridic Crystalline Complex, Northern Italy. J Petrol 28:599–623

Obata M, Ozawa K (2011) Topotaxic relationships between spinel and pyroxene in kelyphite after garnet in mantle-derived peridotites and their implications to reaction mechanism and kinetics. Miner Petrol 101:217–224. https://doi.org/10.1007/s00710-011-0145-y

Obata M, Ozawa K, Naemura K, Miyake A (2013) Isochemical breakdown of garnet in orogenic garnet peridotite and its implication to reaction kinetics. Miner Petrol 107:881–895. https://doi.org/10.1007/s00710-012-0260-4

Palme H, O'Neill HSC (2014) Cosmochemical estimates of mantle composition. In: Turekian K, Holland H (eds) Treatise on Geochemistry, 2nd edn. Elsevier, pp 1–39. https://doi.org/10.1016/B978-0-08-095975-7.00201-1

Pawley A (2003) Chlorite stability in mantle peridotite: the reaction clinochlore + enstatite = forsterite + pyrope + H_2O. Contrib Mineral Petrol 144:449–456. https://doi.org/10.1007/s00410-0409-y

Perraki M, Faryad SW (2014) First finding of microdiamond, coesite and other UHP phases in felsic granulites in the Moldanubian Zone: implications for deep subduction and a revised geodynamic model for Variscan orogeny in the Bohemian Massif. Lithos 202–203:157–166. https://doi.org/10.1016/j.lithos.2014.05.025

Pouchou JL, Pichoir F (1984) A new model for quantitative analyses. I. Application to the analysis of homogeneous samples. La Recherche Aérospatiale 3:13–38

Pouchou JL, Pichoir F (1985) 'PAP' correction procedure for improved quantitative microanalysis. Microbeam Anal 54:104–106

Rey P, Burg J-P, Caron J-M (1992) Middle and Late Carboniferous extension in the Variscan Belt: structural and petrological evidences from the Vosges massif (Eastern France). Geodin Acta 5:17–36

Skrzypek E, Štípská P, Cocherie A (2012) The origin of zircon and the significance of U-Pb ages in high-grade metamorphic rocks: a case study from the Variscan orogenic root (Vosges Mountains, NE France). Contrib Mineral Petrol 164:935–957. https://doi.org/10.1007/s00410-012-0781-1

Sorger D, Hauzenberger CA, Linner M, Iglseder C, Finger F (2018) Carboniferous polymetamorphism recorded in paragneiss–migmatites from the Bavarian Unit (Moldanubian superunit, Upper Austria): implications for the tectonothermal evolution at the end of the Variscan orogeny. J Petrol 59:1359–1382. https://doi.org/10.1093/petrology/egy063

Takahashi E (1986) Melting of a dry peridotite KLB-1 up to 14 GPa: implications on the origin of peridotitic upper mantle. J Geophys Res 91:9367–9382

Thiéry V (2012) La série de la Sioule, 75 ans après les travaux de J. Richard (1938). Historique des études géologiques et évolution des concepts. Revue Des Sciences Naturelles D'auvergne 76:73–91

Tomlinson EL, Holland TJB (2021) A thermodynamic model for the subsolidus evolution and melting of peridotite. J Petrol 62:1–23. https://doi.org/10.1093/petrology/egab012

Vanderhaeghe O, Laurent O, Gardien V, Moyen J-F, Gébelin A, Chelle-Michou C, Couzinié S, Villaros A, Bellanger M (2020) Flow of partially molten crust controlling construction, growth and collapse of the Variscan orogenic belt: the geologic record of the French Massif Central. BSGF Earth Sci Bull 191:25. https://doi.org/10.1051/bsgf/2020013

Vincent PL, Hameurt J, Durand M, Flageollet J-C (1985) Carte géologique de la France à 1/50.000, sheet Bruyères. Ministère du Redéploiement Industriel et du Commerce Extérieur, Service Géologique National

Walter MJ (1998) Melting of garnet peridotite and the origin of komatiite and depleted lithosphere. J Petrol 39:29–60

Webb SAC, Wood BJ (1986) Spinel–pyroxene–garnet relationships and their dependence on Cr/Al ratio. Contrib Mineral Petrol 92:471–480

Whitney DL, Evans BW (2010) Abbreviations for names of rock-forming minerals. Am Mineral 95:185–187. https://doi.org/10.2138/am.2010.3371

Zhang J, Herzberg C (1994) Melting eperiments on anhydrous peridotite KLB-1 from 5.0 to 22.5 GPa. J Geophys Res 99:17729–17742

Ziberna L, Klemme S, Nimis P (2013) Garnet and spinel in fertile and depleted mantle: insights from thermodynamic modelling. Contrib Mineral Petrol 166:411–421. https://doi.org/10.1007/s00410-013-0882-5